1-1-2017

Targeting Host Defense: The Dynamic Nd10 Interaction And The Differential Substrate Recognition Of Hsv-1 Icp0

Yi Zheng
Wayne State University,

TARGETING HOST DEFENSE: THE DYNAMIC ND10 INTERACTION AND THE DIFFERENTIAL SUBSTRATE RECOGNITION OF HSV-1 ICP0

by

YI ZHENG

DISSERTATION

Submitted to the Graduate School

of Wayne State University,

Detroit, Michigan

in partial fulfillment of the requirements

for the degree of

DOCTOR OF PHILOSOPHY

2017

MAJOR: BIOLOGICAL SCIENCES

Approved By:

_____

Advisor   Date

_____

_____

_____

_____

DEDICATION

To my parents and my friends:

Thanks for your support through this long journey!

ACKNOWLEDGMENTS

First and foremost, I would like to express my gratitude to Dr. Haidong Gu. I am extremely lucky to do my research under her mentorship. Over the past five years, she has guided me to carry out productive research and taught me the approach to ask important questions and interpret complex results. She always supported me to present my work at symposiums and conferences and helped me to improve my presentation skills. I hope to have her guidance for the rest of my scientific career. Thank you very much, Dr. Gu.

Next, I extend my appreciation to my committee members. Dr. Lori Pile has given me a lot of valuable suggestions on my research and career. I want to thank Dr. Miriam Greenberg for her constructive criticisms during committee meetings. I am thankful to Dr. Philip Pellett for his suggestions on my presentation, writing and research projects.

I also want to thank all my previous and current lab members. Particular acknowledgments go to Subodh Samrat for constructing the cell lines for my second project and Lisa Li for proofreading my thesis.

I extend my gratitude to chromatin journal club members, molecular biology division members for their valuable suggestions. I am thankful to all the professors who taught me during my courses. I also extend my thankfulness to Dr. Edward Golenberg and the staffs in the Biological Science Department for helping me out with documentation and paperwork.

Last but not the least, I appreciate the support of the closest people in my life. My parents are always supportive of my study and research. I also want to appreciate the encouragement from my previous teachers Dr. Minhua Luo and Dr. Min Hu, who are

always caring about my research career. My friends Honghu Quan, Duong Nguyen, and Feng Tao are always encouraging me when I feel frustrated. I truly appreciate the help and support from my friends.

TABLE OF CONTENTS

LIST OF TABLES

LIST OF FIGURES

CHAPTER 1 INTRODUCTION

HSV-1 overview

Herpes simplex virus 1 (HSV-1), also known as human alphaherpesvirus 1 (HHV-1), belongs to *Herpesviridae*. HSV-1 is ubiquitous, infecting over 70% of the world population. It is transmitted through direct contact with infected people who are producing and shedding the virus. HSV-1 infections cause a broad range of mild to severe herpetic diseases, including cold sores, genital lesions, stromal keratitis, and encephalitis (Roizman et al., 2013).

A complete HSV-1 virion contains four distinct structures: core viral DNA, capsid, tegument, and envelope. HSV-1 genome is encased within an icosahedral capsid, which is then wrapped in a lipid bilayer envelope. Between the envelope and capsid is a proteinous layer called tegument. Tegument contains at least 20 proteins and has diverse functions, involved in entry, egress, transcription and translation regulation, and immune modulation (Kelly et al., 2009). HSV-1 has a 152 kb linear and double-stranded DNA genome, which has unique long (UL) and unique short (US) regions, flanked by inverted repeats. HSV-1 has a great coding capacity, encoding at least 84 viral proteins (Roizman et al., 2013).

HSV-1 establishes either lytic or latent infection depending on the cell types. Lytic infection mainly occurs in the epithelial cells, while the latent viral DNA resides in the trigeminal ganglia (Knipe and Cliffe, 2008). The lytic life cycle of HSV-1 includes entry, uncoating, gene expression, genome replication, assembly, and egress. Entry of virion particles to the host cell initiates through the reversible binding of viral glycoproteins to the glycosaminoglycans (GAG) located on the cell surface (WuDunn and Spear, 1989).

HSV-1 then enters into cells through either fusion or endocytosis. Following entry, capsids containing viral DNA are released into the cytoplasm, translocated to the nuclear pore along the microtubule network, and docked at the nuclear pore (Kristensson et al., 1986). Afterward, the viral DNA is released from the capsid into the nucleus (Batterson et al., 1983). RNA pol II of the host cell is responsible for the transcription of viral DNA in the nucleus (Costanzo et al., 1977). Viral gene expression is a tightly regulated cascade, including immediate-early (α), early (β), and late (γ) stages. Immediate early (α) genes include α0, α4, α 27, α22, and α47 that express soon after infection (Roizman et al., 2013). At approximately 2 to 4 hours post infection (hpi) at 10 or 20 pfu/cell, α proteins are synthesized at the highest rate (Honess and Roizman, 1974). The tegument protein VP16 recruits host cell factor 1 (HCF-1) and octamer transcription factor 1 (Oct-1) to boost α promoter activity and stimulate the transcription of α genes that does not require *de novo* viral protein synthesis (Wysocka and Herr, 2003). α proteins activate the transcription of β genes, which are independent of viral DNA synthesis. β proteins, which are involved in viral DNA replication and nucleotide metabolism, are expressed at the highest rate between about 4 to 8 hpi (Honess and Roizman, 1974). γ gene transcription is enhanced upon the viral genome replication. γ genes are divided into two groups, γ_1 (leaky late) and γ_2 (true late). γ proteins are predominantly involved in the assembly of the progeny virions.

Following lytic infection in epithelial cells, viral particles enter nerve termini and are delivered into the nucleus of sensory neurons through retrograde transport to establish latent infection (Knipe and Cliffe, 2008). During latency, HSV-1 genome persists as a non-integrated, circular, and histone-associated episome. Transcription of viral lytic genes is suppressed through the epigenetic process. Nucleosomes at promoters of lytic genes are

enriched with the facultative heterochromatin marker H3K27 trimethylation (Bloom et al., 2010). Different from the lytic genes, the promoter of latency-associated transcript (LAT) possesses active markers for transcription, such as H3K4 dimethylation and H3K9, K14 acetylation. Consistent with this, LAT is actively transcribed during the latency stage. Deletion of LAT does not eliminate the presence of latent viral DNA in mouse ganglia (Ho and Mocarski, 1989), suggesting LAT is not essential for the establishment of latency. LAT expression can promote the heterochromatin assembly on the promoters of lytic genes, indicating the participation of LAT in the regulation of latency maintenance (Wang et al., 2005).

Periodically, the latent viruses are reactivated to a lytic state under hormonal, physical, or emotional stress. Newly synthesized virions are transported in an anterograde manner to epithelial cells where they initiate productive infection (Knipe and Cliffe, 2008). A recent study proposes a reactivation model involving two phases (Kim et al., 2012). During phase I of reactivation, random expression of all α, β, and γ genes occurs without VP16 in the nucleus (Cliffe and Wilson, 2017). In Phase II, VP16 translocates to the nucleus to transactivate transcription of α genes and the regulated cascade of α, β, and γ gene expression is restored. Phase II culminates in the production of infectious virus (Kim et al., 2012).

ICP0 overview

Infected cell protein 0 (ICP0), encoded by the diploid α0 gene, is one of the immediate early viral proteins. ICP0 is essential for viral replication in low multiplicity of infection (MOI) but is dispensable at high MOI (Chen and Silverstein, 1992), suggesting ICP0 executes its functions through saturating cellular factors. ICP0 is a trans-acting

transcriptional activator (Everett, 1987). C3HC4 zinc binding really interesting new gene (*RING*) finger motif located in the N-terminus of ICP0 is critical for its transactivation function (Chen et al., 1991). Conserved RING finger sequences are present in a large family of E3 ubiquitin ligases (Freemont, 2000), and ICP0 has been proven to be a RING-dependent E3 ubiquitin ligase (Boutell et al., 2002).

The earliest identified substrates of ICP0 are the Nuclear Domain 10 (ND10) components, promyelocytic leukemia protein (PML) and Sp100 (Chelbi-Alix and de The, 1999). Besides PML and Sp100, substrates of ICP0 also include ubiquitin-specific-processing protease 7 (USP7), ring finger protein 8 (RNF8), ring finger protein 168 (RNF168), and DNA-dependent protein kinase catalytic unit (DNA-PKcs) (Boutell et al., 2005; Lees-Miller et al., 1996; Lilley et al., 2010). In addition to serving as E3 ligase, ICP0 also interacts with multiple cellular proteins. For example, residue D199 of ICP0 binds with cyclin D3, and residues D671/E673 of ICP0 are responsible for association with CoREST (Fig 1.1). The substrates and binding partners of ICP0 are involved in various cellular pathways, including immune evasion, chromatin remodeling, DNA damage response, and ubiquitin-proteasome pathway. By attenuating multiple pathways simultaneously, ICP0 counteracts the host antiviral response to enhance the viral gene expression (Gu, 2016).

Fig 1.1: Functional domains in ICP0. RING stands for the RING finger motif containing E3 ligase activity. T67 binds to RNF8, D199 binds to Cyclin D3 and D671/E673 bind to CoREST. Residues 620-626 of ICP0 are responsible for binding with USP7. SUMO interaction motif (SIM$_{362-364}$) and nuclear localization signal (NLS) are also illustrated.

ICP0 is essential for HSV-1 to counteract the interferon (IFN) response, and HSV-1 with mutant ICP0 is hypersensitive to IFN treatment (Mossman et al., 2000). ICP0 contributes to resistance to IFN in multiple aspects. First, ICP0 can efficiently degrade PML. PML (+/+) cells reduce ICP0 null virus 1,000 fold more than PML (-/-) cells under IFN treatment (Chee et al., 2003); however, the difference is minimal for wild-type virus, suggesting that ICP0 destroys PML to attenuate PML mediated innate immunity. Second, ICP0 is responsible for proteasomal degradation of interferon gamma inducible protein 16 (IFI16) (Orzalli et al., 2012), a double-stranded viral DNA sensor that elicits the downstream interferon regulatory factor 3 (IRF3)-dependent IFN response. Degradation of IFI16 leads to inactivation of IRF3 and alleviates subsequent IFN response. Third, ICP0 can sequester activated IRF3 and histone acetyltransferase p300 in ICP0 nuclear foci, preventing their association with promoters of IFN stimulated genes (ISGs) and activation of IFN response (Melroe et al., 2007). The fact that ICP0 utilizes multiple mechanisms to abrogate IFN response emphasizes the importance of counteracting IFN response for efficient viral infection.

ICP0 also remodels chromatin associated with the HSV-1 genome for efficient viral gene expression. The injected HSV-1 DNA is histone free, but histone H3 is found on viral DNA as early as 1 hpi (Oh and Fraser, 2008). Histone depositions on DNA impede the transcription (Li et al., 2007). Viral proteins VP16 and ICP0 are responsible for the removal and remodeling of the histones associated with viral DNA. Tegument protein VP16 mainly stimulates the expression of α genes (Herrera and Triezenberg, 2004), while ICP0 is primarily responsible for activating the expression of β and γ genes. ICP0 reduces the presence of H3 together with repressive heterochromatin markers on HSV-1 genome

and increases the acetylation level on the promoters of β and γ genes (Cliffe and Knipe, 2008). Several activities suggest a chromatin remodeling function of ICP0. First, ICP0 interacts with repressive transcription regulators to inhibit their function. ICP0 can bind with class II HDAC4, 5, and 7 to attenuate their function in a reporter assay (Lomonte et al., 2004). Moreover, ICP0 also interacts with CoREST to disassociate HDAC1 from CoREST and REST complex (Gu et al., 2005). Second, ICP0 cooperates with transcription activator. ICP0 can interact with RanBP10, a transcription coactivator, to promote viral gene expression by decreasing the H3 level on the viral genome (Sato et al., 2016). Third, ICP0 degrades restrictive factors that repress viral gene expression. The intrinsic immunity effector IFI16 promotes the heterochromatin deposition on the viral genome. Degradation of IFI16 by ICP0 leads to more euchromatin and less heterochromatin associated with viral genome (Orzalli et al., 2013). In summary, ICP0 remodels the repressive chromatin on viral DNA through various strategies, which underlines its significance in enhancing viral gene expression.

HSV-1 also modulates DNA damage response (DDR). Mismatch repair (MMR) proteins relocalize to viral replication compartments and are required for efficient viral replication (Mohni et al., 2011). In addition to MMR, HSV-1 also manipulates double-strand DNA break repair including classic non-homologous end joining (C-NHEJ) and homologous recombination (HR) (Smith and Weller, 2015). ICP0 is responsible for attenuating both pathways. ICP0 inhibits C-NHEJ by depleting the level of the DNA-PKcs during HSV-1 infection without affecting Ku70/80 activity (Lees-Miller et al., 1996). Wild-type HSV-1 and ICP0 null viruses have a mild decrease of replication in DNA-PK positive cells compared with in DNA-PK negative cells, suggesting DNA-PK has an inhibitory role in viral DNA

replication. In addition to DNA-PKcs, two E3 ubiquitin ligases RNF8 and RNF168 involved in HR are also targeted by ICP0. ICP0 can polyubiquitinate RNF8 and RNF168 in the RING-dependent manner for subsequent proteasomal degradation (Lilley et al., 2010). Moreover, RNF8 inhibits the plaque formation of ICP0 null virus, suggesting it is a restrictive factor for viral replication (Lilley et al., 2011). However, it needs to be noticed that several components of HR machinery such as ATM and MRN are critical for efficient viral production (Lilley et al., 2005). Overall, HSV-1 exploits the beneficial DDR machinery and eliminates the inhibitory DDR components. ICP0 is mainly utilized to target the restrictive factors in the DDR pathway for proteasomal degradation to relieve their repression on viral replication.

ICP0 is also involved in regulation of the ubiquitin-proteasome pathway through strong association with USP7, which has been shown to promote USP7 polyubiquitination through *in vitro* ubiquitination assay (Canning et al., 2004). Consistent with this, the ICP0-USP7 interaction is required for the degradation of USP7 by ICP0 in infected cells (Boutell et al., 2005). Presumably, the interaction with USP7 inhibits autoubiquitination of ICP0 and promotes the viral infection by enhancing ICP0 stability. This idea is supported by a report from one group (Boutell et al., 2005); however, another group has indicated that wild-type ICP0 turns over quickly shortly after infection regardless of USP7 binding (Gu et al., 2009). In addition, a mutant virus, in which ICP0 is unable to bind USP7, has enhanced, not reduced, viral gene expression (Kalamvoki et al., 2012). Therefore, the actual role of USP7 interaction with ICP0 during viral infection still needs further investigation.

Overall, ICP0 attacks various substrates in diverse cellular pathways to achieve the

transactivation of viral gene expression. As a result, an interesting question is how ICP0 can target them simultaneously. Disrupting nuclear structures ND10 can be part of the solution. ND10 are closely connected with multiple pathways, including transcriptional regulation (Zhong et al., 2000), apoptosis (Bernardi and Pandolfi, 2003), DNA damage response (di Masi et al., 2016), oncogenesis (Salomoni and Pandolfi, 2002), and antiviral response (Everett and Chelbi-Alix, 2007). Some of these pathways overlap with the cellular pathways ICP0 counteracts. During infection, HSV-1 viral DNA is in close proximity to ND10 (Maul et al., 1996). ND10 restrict viral gene expression, and HSV-1 employs ICP0 to destroy the inhibitory function of ND10 (Everett et al., 2006). Therefore, the interaction between virus and ND10 is of biological significance for viral infection.

ND10 (PML-NB) components, structure, and antiviral functions

ND10 are punctate structures found in the nuclei (Ascoli and Maul, 1991). The structure of ND10 is usually described as doughnout-shaped based on confocal laser-scanning microscopy (CLSM) and electron microscopy (EM) (Bernardi and Pandolfi, 2007). Each ND10 structure contains a shell and an inner core (Lang et al., 2010). Since PML is the chief organizer for ND10 and required for ND10 formation, ND10 are also called PML nuclear bodies (PML-NBs). Besides PML, constitutive components of ND10 also include Sp100, Death-associated protein 6 (Daxx), and ATP-dependent helicase ATRX (Negorev and Maul, 2001). Until now, more than 150 cellular proteins have been identified as ND10 components (Van Damme et al., 2010), while many are recruited upon certain stimulations (Bernardi and Pandolfi, 2007). PML has seven isoforms. PML isoform V has the longest residence time and least turnover dynamics, suggesting that PML isoform V is the scaffold protein of ND10 (Weidtkamp-Peters et al., 2008). The same study also

found that all PML isoforms and Sp100 have slower dynamics compared with Daxx, Bloom syndrome protein (BLM), and Homeodomain-interacting protein kinase 2 (HIPK2). This phenomenon is consistent with the fact that PML and Sp100 are the organizers of ND10, while others are highly dynamic and transiently recruited to ND10.

ND10 nuclear bodies consist of numerous constant and transiently recruited proteins and consequently, are attributed to various biological functions including transcriptional regulation, apoptosis, DNA repair, and oncogenesis (Lallemand-Breitenbach and de The, 2010). ND10 components are also involved in antiviral response including both intrinsic and innate immunity. Unlike innate immune responses, intrinsic immunity consists of restrictive proteins that are usually expressed at constant levels and can halt viral infection immediately (Yan and Chen, 2012). Several clues support ND10 involvement in intrinsic immune response. First, stable overexpression of PML inhibits replication of vesicular stomatitis virus (VSV) and influenza virus (IAV) (Chelbi-Alix et al., 1998). Second, PML utilizes diverse mechanisms including both protein-protein interaction and chromatin remodeling to regulate the intrinsic antiviral response. PML interacts with a retroviral transactivator Tas and prevents its binding to viral DNA, which leads to a drastic decrease of human foamy virus (HFV) protein expression (Regad et al., 2001). Another study demonstrated that stable overexpression of PML affects the early stage of HIV replication, which can be reversed by the histone deacetylase (HDAC) inhibitor SAHA, suggesting that the intrinsic antiviral ability of PML is likely through regulating the heterochromatin deposition on the viral genome (Maroui et al., 2011). Third, components of ND10 cooperatively mount the intrinsic antiviral response. The depletion of PML, together with Sp100 and Daxx can enhance the ICP0 null viral yield more significantly

than a single knockdown of PML (Glass and Everett, 2013).

Besides regulating intrinsic immunity, ND10 also participate in innate immunity. IFN, secreted mainly by the dendritic cells, plays a central role in innate immunity (Turvey and Broide, 2010). The evidence connecting ND10 with innate immunity originates from the observation that IFN treatment increases the expression of PML and Sp100, together with the intensity and the numbers of ND10 (Lavau et al., 1995). Besides, PML knockout cells reduce the capacity of IFN in restricting viral infections, suggesting that PML plays a significant role in the establishment of an IFN-induced antiviral state (Chee et al., 2003). A recent study indicates that PML stimulates expression of the ISGs to enhance the type I IFN response. Specifically, PML interacts with interferon-stimulated gene factor 3 (ISGF3), signal transducer and activator of transcription 1 (STAT1), and signal transducer and activator of transcription 2 (STAT2) to positively regulate the ISG promoter activity (Kim and Ahn, 2015). These phenomena implicate that PML and IFN form a positive feedback in mediating innate immunity to mount antiviral state. Overall, ND10 components are associated with both intrinsic and innate immunity to restrict viral infection.

HSV-1 ICP0 and ND10

Upon infection, HSV-1 viral DNA is injected into the nucleus and found to be closely associated with ND10 (Maul et al., 1996). Since ND10 nuclear bodies mediate both intrinsic and innate immunity, the close association between ND10 and viral genome causes the repression of viral gene expression. ICP0, after its synthesis, localizes to ND10 (Maul et al., 1993) and uses its E3 ligase activity to degrade PML and Sp100 (Chelbi-Alix and de The, 1999). Since PML and Sp100 are the main organizers for ND10

formation, the degradation of PML and Sp100 leads to the dispersal of the inimical ND10 components and subsequent derepression of the HSV-1 genome (Everett et al., 2006).

Even though HSV-1 uses ICP0 to dismantle ND10 and alleviate viral gene expression, the interesting phenomenon is that HSV-1 starts its replication in the proximity to ND10 (Uprichard and Knipe, 1997). Two reasons may explain why HSV-1 has such an intimate relationship with ND10. One is that HSV-1 needs to degrade restrictive factors in ND10 for efficient viral gene expression. For example, Sp100 knockdown greatly increases the viral plaque formation and viral gene expression of ICP0 null virus, whereas the effect is minimal for wild-type virus (Everett et al., 2008). The other is that HSV-1 also takes advantage of ND10 components that are beneficial for viral replication. For instance, MLH1, a mismatch repair protein and one of the ND10 components, is recruited to viral replication compartment and required for efficient viral replication (Mohni et al., 2011). Recently, an interesting study found that PML plays both inimical and beneficial role in HSV-1 replication (Xu et al., 2016). This study is consistent with the idea that HSV-1 destroys the restrictive components and gathers the favorable constituents from ND10 for efficient viral replication.

In addition to herpesvirus, other viral families including adenovirus, polyomavirus, simian virus 40 (SV40), as well as papillomavirus also destroy ND10 and initiate their replication near ND10, suggesting exploiting ND10 is a common strategy for efficient viral replication in the nucleus (Tavalai and Stamminger, 2008). Therefore, deciphering the interaction between HSV-1 and ND10 is significant for understanding DNA virus replication in general.

As aforementioned, ICP0 localizes to ND10 (Maul et al., 1993) after its synthesis and

degrades PML and Sp100 (Chelbi-Alix and de The, 1999; Everett et al., 1998) during infection. Our lab investigated the interaction between ICP0 and ND10 and have found that there is a dynamic association between ICP0 and ND10 (Gu et al., 2013), which includes three sequential steps, adhesion, fusion, and retention (Fig 1.2).
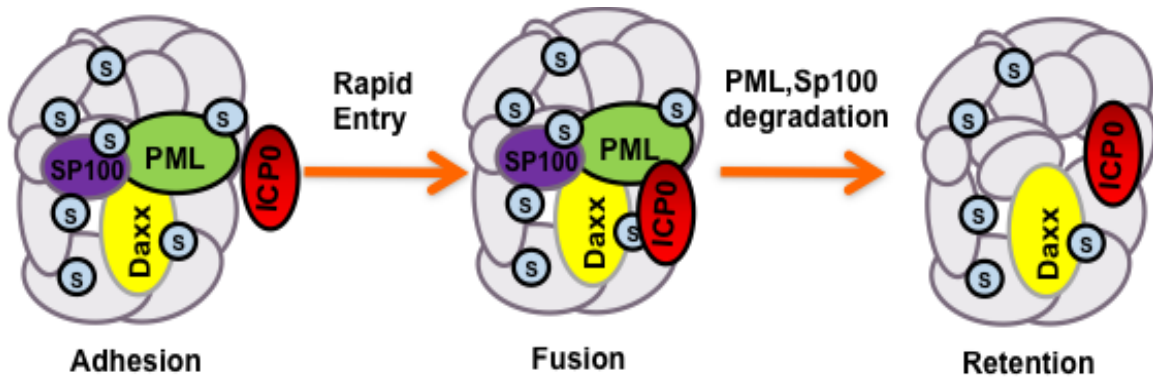
Fig 1.2: Dynamic interaction between ICP0 and ND10 include three steps: adhesion, fusion, and retention. Wild-type ICP0 adheres to the surface of ND10. This is a transient process that quickly leads to the fusion of ICP0 to ND10 bodies. PML and Sp100 are degraded, while ICP0 is retained at ND10. ND10 is subsequently dispersed.

Specific ICP0 domains are involved in each of the three phases. ICP0 with deletion of residues 245 to 474 fails to colocalize with ND10 (fusion). Therefore, our lab defines residues 245 to 474 of ICP0 as the ND10 entry sequence (ND10-ES), which is responsible for ND10 fusion process. The dynamic interaction between ICP0 and ND10 suggests that ICP0 may bind with a distinct group of ND10 constituents in each step to manipulate ND10 and enhance viral replication. The ND10 fusion step possibly controls ICP0 access to its inhibitory substrates. In the meantime, ICP0 can interact with beneficial ND10 components to enhance viral replication at this step. Characterization of ND10-ES is the necessary groundwork for delineating protein-protein interactions during ND10 fusion process. In Chapter 2, I focus on characterizing the molecular features of ND10-

ES and determining the minimum sequence requirement for ICP0-ND10 fusion.

Ubiquitination in modulation of viral infection

As aforementioned, ICP0 participates in multiple cellular pathways and targets various substrates for ubiquitination and proteasomal degradation. Knockdown of ICP0 substrates mentioned above can increase viral gene expression and replication to different extents (Gu, 2016), indicating that these substrates are part of the antiviral defense. An interesting question is how ICP0 can manipulate so many substrates to achieve the counteraction of host antiviral response. To answer this question, I used sample substrates to investigate the ICP0 functional domains that are responsible for the recognition and ubiquitination of different substrates.

Ubiquitin is an 8.5 kDa protein composed of 76 amino acids. Ubiquitination is one of the post-translational modifications and is completed through three distinct classes of enzymes (Pickart and Eddins, 2004). The ubiquitin-activating enzyme (E1) initiates the activation of ubiquitin by binding to its C-terminus, which requires ATP. The activated ubiquitin on E1 is then transferred to a second protein, the ubiquitin-conjugating enzyme (E2). The E2 protein acts in conjunction with ubiquitin ligase (E3), which binds to the substrate protein and catalyzes the transfer of ubiquitin to a lysine on the substrate protein. Since there are limited numbers of E1 and E2 enzymes, the substrate specificity relies mainly on the E3 ubiquitin ligase enzymes. E3s are divided into three types, HECT (homologous to E6-associated protein C-terminus), RING (Really Interesting New Gene), and RBR (RING-in-between-RING) (Zheng and Shabek, 2017). The main differences between these E3s are how they ubiquitinate their substrates. For HECT and RBR types, ubiquitin is transferred from E2 to the cysteine residue of E3 first before ubiquitin molecule

is transferred to the substrates. Distinct from HECT and RBR E3 ligases, the ubiquitin molecule is directly transferred from E2 to substrates without the middle transition in RING-type E3 ligases (Zheng and Shabek, 2017).

Conjugation of ubiquitin to the substrate occurs at lysine residues. Lysine residues of the substrate can be modified with a single ubiquitin moiety (monoubiquitination) or chains of ubiquitin (polyubiquitination). Polyubiquitin chains are formed through the covalent binding of C-terminal glycine of one ubiquitin molecule with the lysine or methionine of another ubiquitin molecule (Pickart and Eddins, 2004). Ubiquitin itself contains eight amino groups for another ubiquitin molecule to conjugate with: the ε-amino groups of seven lysine residues (K6, 11, 27, 29, 33, 48, and 63) and the α-amino group of the N-terminal methionine residue. Among them, the K48- and K63-linked chains are the most abundant and the best described. K48-based polyubiquitin chain leads to the proteasome-dependent degradation, while K63-based chain regulates protein endocytosis, trafficking, and enzymatic activity (Yau and Rape, 2016). In contrast to homotypic chains, the heterotypic ubiquitin chains are made up of mixed and branched linkages. The heterotypic chains have been reported to involve in the proteolytic and innate immunity signaling pathway (Deng et al., 2000; Meyer and Rape, 2014).

The ability of ubiquitin to form structurally and functionally distinct polymers greatly increases the complexity of ubiquitination. Since different types of ubiquitin linkages are associated with distinct functions (Welchman et al., 2005), viruses also exploit and modulate these biological functions of ubiquitination to facilitate their infection. Ubiquitin system is utilized by viruses to target host immune adaptor and signaling molecules to achieve immune evasion. Viruses either possess their E3 ubiquitin ligases or hijack the

cellular E3 ubiquitin ligase complex to degrade immune adaptor. As aforementioned, HSV-1 encodes ICP0, which is the RING-dependent E3 ligase, for proteasomal degradation of multiple cellular proteins to suppress intrinsic and innate immunity. Hijacking cellular E3 ligases is another common mechanism for viruses to suppress the host immune responses. Non-structural protein 1 (NSP1) of rotavirus, an interferon (IFN) antagonist, promotes virus replication by mediating the degradation of antiviral factors including IRF3 and β-TrCP (Arnold, 2016). The strain-specific NSP1 associates with cellular Cullin-1 (Cul1) and Cullin-3 (Cul3) and employs RING-box protein 1 (Rbx1) E3 ligase activity to degrade β-TrCP and inactivate the NF-κB pathway (Ding et al., 2016).

In addition to the modulation of host cell immunity, every single step in viral life cycle including entry, uncoating, genome replication, and egress is also under the regulation of ubiquitination. Proteasome inhibitors including MG132 and lactacystin can effectively interfere with viral entry and intracellular trafficking (Greene et al., 2012; Wang et al., 2016), suggesting that a functional ubiquitin-proteasome system is critical for productive entry process. Ubiquitination can enhance both viral genome replication and viral egress through two mechanisms. First, ubiquitination stimulates the function of viral polymerase and proteins essential for egress directly. For example, ubiquitination of viral polymerase subunits stimulates their function to enhance viral genome replication during influenza virus (IAV) infection (Hrecka et al., 2011; Kirui et al., 2016). Human immunodeficiency virus (HIV) virions contain both free ubiquitin and ubiquitinated Gag, suggesting that ubiquitination is part of HIV budding machinery (Ott et al., 1998; Patnaik et al., 2000). Recent findings found that Gag fused with the active deubiquitinase (DUB) domain of UL36 from HSV-1 cannot support the virus release, indicating that ubiquitination of Gag

is critical for HIV budding (Sette et al., 2013). Second, ubiquitination is utilized to degrade the host factors restricting viral replication and egress. For instance, viral protein HBx associates with DDB1-CUL4-ROC1 (CRL4) E3 ligase complex to degrade SMC5 and SMC6 in hepatitis B virus (HBV) infection. Degradation of SMC5 and SMC6 relieves their inhibition on HBV genome replication (Decorsiere et al., 2016; Murphy et al., 2016). BST-2 (Tetherin) is an intrinsic restriction factor that blocks the release of newly generated HIV viral particles from the infected cell membrane (Perez-Caballero et al., 2009). In HIV, Vpu recruits β-TrCP to polyubiquitinate and degrades BST-2, which releases the viral particles from the plasma membrane for viral dissemination (Mitchell et al., 2009).

Overall, ubiquitination is extremely important in regulating viral counteraction of host immune response and viral life cycle. Viruses manipulate and utilize ubiquitination to enhance viral gene expression and viral infection. In Chapter 3, I focus on identification of ICP0 elements regulating its E3 ligase activity and substrate recognition.

CHAPTER 2 IDENTIFICATION OF THREE REDUNDANT SEGMENTS RESPONSIBLE FOR HSV-1 ICP0 TO FUSE WITH ND10 NUCLEAR BODIES

Introduction

During HSV-1 lytic infection, viral DNA is injected into the nucleus and located near ND10 nuclear bodies (Maul et al., 1996). As aforementioned, ND10 nuclear bodies mediate both intrinsic and innate immunity. The close association between ND10 and viral genome causes the repression of viral gene expression. After its synthesis, ICP0 localizes to ND10 (Maul et al., 1993) and uses its RING-type E3 ubiquitin ligase to ubiquitinate PML and Sp100 for proteasomal degradation (Chelbi-Alix and de The, 1999). Degradation of PML and Sp100, key organizers of ND10, leads to dispersal of ND10 components and subsequent derepression of the HSV-1 genome (Everett et al., 2006). Recombinant virus carrying ICP0 with mutations in RING finger motif, which is incapable of destroying ND10, showed impaired viral growth in BHK fibroblast cells (Everett et al., 1995). A combinational depletion of several ND10 components, including PML, Sp100, and Daxx, can increase ICP0 null virus replication much more significantly than wild-type ICP0 virus (Glass and Everett, 2013). These phenomena suggest that inactivation of inhibition from ND10 components by ICP0 is critical for efficient viral gene expression and replication.

During infection, ICP0 has a dynamic movement. ICP0 first localizes to ND10 (Maul et al., 1993). Then ICP0 leads to the proteasomal degradation of ND10 proteins PML and Sp100 (Chelbi-Alix and de The, 1999; Everett et al., 1998). Degradation of PML leads to the dispersal of ND10, and ICP0 diffuses throughout the nucleus subsequently (Maul and Everett, 1994). Later on, ICP0 disappears from the nucleus and translocates to the cytoplasm (Everett and Maul, 1994). The dynamic trafficking of ICP0 is likely involved in coordinating the interactions between ICP0 and its multiple targets. To delineate ICP0 functions, our lab chose to investigate the first event, ICP0 interaction with ND10. We have demonstrated that the interaction between ICP0 and ND10 is a dynamic process, which includes three sequential steps: adhesion, fusion, and retention (Gu et al., 2013). Upon synthesis, ICP0 adheres at the ND10 surface and then rapidly fuses with the ND10 body (Gu et al., 2013). The adhesion phase is very transient. Therefore, only the merged status can be observed for wild-type ICP0, which was previously defined as ICP0-ND10 colocalization (Maul and Everett, 1994). We have identified residues 245 to 474 of ICP0 as the ND10 entry sequence (ND10-ES) responsible for ND10 fusion step (Gu et al., 2013). Deletion of the ND10-ES blocks ICP0 from merging into ND10 after adhering at the ND10 surface, which shows ICP0 in juxtaposition with ND10, instead of colocalization with ND10. C-terminus of ICP0 is responsible for ND10 retention. ICP0 with deletion of C-terminus is dispersed throughout the nucleus. These novel findings redefine the prior static description of ICP0-ND10 colocalization (Maul et al., 1993) and support the idea that ICP0 may interact with a distinct group of ND10 components in each step to execute its function.

The ND10 fusion step presumably regulates ICP0 to approach and degrade its

inhibitory substrates. Meanwhile, ICP0 can catch beneficial ND10 components for efficient viral replication at this stage. Therefore, ICP0 fusion with ND10 is likely a critical step for regulating functions of ICP0. To understand how ND10 fusion step controls functions of ICP0, a thorough characterization of ICP0 motif responsible for fusion is necessary for delineating ICP0 interaction with other proteins. In this chapter, I focus on determining the minimum sequence requirement for ICP0-ND10 fusion. Through deletion mapping and confocal microscopy, I have found that there are three redundant segments located in ND10-ES responsible for the ND10 fusion process. Each of them is competent for driving fusion. The fusion of ICP0 with ND10 will be blocked only when all three ND10 fusion segments are deleted simultaneously.

Material and Methods

Cells

Immortalized human embryonic lung (HEL) fibroblasts received from Thomas E. Shenk (Princeton University) and HEp-2 cells were grown in Dulbecco's modified Eagle's medium (DMEM) supplemented with 10% fetal bovine serum (FBS). Human osteosarcoma U2OS cells from ATCC were cultured in McCoy's 5A medium (Invitrogen) supplemented with 10% FBS.

Viruses

The construction of recombinant viruses RHG101, 110, and 120 have been described elsewhere (Gu et al., 2013). Within all plasmids and recombinant viruses, Dr. Haidong Gu constructed pHG111 to pHG114, pHG121, RHG 111 to RHG114, and RHG121 before I joined the lab. I constructed the remaining plasmids and recombinant viruses. A two-round PCR strategy was adopted to construct RHG115, RHG122 to RHG126, and

RHG130. The pairs of forward and reverse primers designed for each mutant are complementary to each other (detailed primer information is listed in Table 2.1). Each primer has 20 to 30 nucleotides upstream of the deletion or mutation junction directly connected to the 20 to 30 nucleotides downstream of the deletion or mutation junction. In the first round of PCR, forward primers were paired with a downstream primer, 5′-GCAGTCGACTTACCCGGGCCCACCCTGGCCGCG-3′, and reserve primers were paired with an upstream primer, 5′-GCAGGATCCGCGGTCTCGGGGGGGAGC-3′, to amplify the fragments downstream or upstream of the deletion or mutation junction, respectively. In the second round of PCR, we used purified upstream and downstream PCR products as the template to amplify the joined fragments containing the designated internal deletions or mutations. These deletion or mutation products were digested with XhoI and MluI to swap the fragment between the XhoI and MluI sites of plasmid pHG101, in which an mCherry-tagged full-length ICP0 cDNA is flanked by the 5′ and 3′ ICP0-flanking sequences from the HSV-1 (F) genome. The plasmids obtained were named pHG115, pHG122 to pHG126, and pHG130 corresponding to the virus names.

To substitute ICP0 residues 245 to 474 with varicella-zoster virus (VZV) ORF61 corresponding region, primers 5′-CTGGACGACGCAGACTACAGATCTGATATCGGGCCCTCCCGCGGCGCC-3′ and 5′-GGCGCCGCGGGAGGGCCCGATATCAGATCTGTAGTCTGCGTCGTCCAG-3′ were used to generate BglII and EcoRV sites between the junction of amino acids 244 and 475 of ICP0 according to the two-round PCR strategy described above. VZV ORF61

primers 5′-CGCGGATCCGATCTTCTGCCACCAAGC-3′ and 5′-ACGGATATCTGTATCTTTCCAGGTCCA-3′ were used to amplify ORF61 amino acids

105 to 335. The plasmid pcDNA3.1 (+)-VZV ORF61, a generous gift from Dr. Ann Arvin (Stanford University), was used as the template. The PCR product containing ORF61 residues 105 to 335 was digested with BamHI and EcoRV and inserted into the BglII and EcoRV sites as described above.

Table 2.1: Primers for ICP0 internal deletions or mutations

Viruses		Primer sequences
RHG114	Forward	5'-GGCTCCGCCCCCCGCCCCGGGCCCCCCGCGTCCTCGTCCCTGGCTCAGGCCGCGAACCAAGAACAGAGT-3'
	Reverse	5'-ACTCTGTTCTTGGTTCGCGGCCTGAGCCAGGGACGAGGACGCGGGGGGCCCGGGGCGGGGGGCGGAGCC-3'
RHG115	Forward	5'-GTGCCCCAGTCGCACTCGGGGCCCTCCCGCGGCGCC-3'
	Reverse	5'-GGCGCCGCGGGAGGGCCCCGAGTGCGACTGGGGCAC-3'
RHG121	Forward	5'-CACCACGGACGAGGATGACGACGACCTGGACGACAGGGGCCGGACGGGCCCCCTTGTCAACAGACCC-3'
	Reverse	5'-GGGTCTGTTGACAAGGGGGCCCGTCCGGCCCCTGTCGTCCAGGTCGTCGTCATCCTCGTCCGTGGTG-3'
RHG122	Forward	5'-GCGCCCATCGGGCCACACTCCGCGGCCGCGTCGGGA-3'
	Reverse	5'-TCCCGACGCGGCCGCGGAGTGTGGCCCGATGGGCGC-3'
RHG123	Forward	5'-GAGGCGGGGCGGCCGAGGTCGTCCCTGGCTCAGGCC-3'
	Reverse	5'-GGCCTGAGCCAGGGACGACCTCGGCCGCCCCGCCTC-3'
RHG124	Forward	5'-GACGACGACCTGGACGACTCCGCGGCCGCGTCGGGA-3'
	Reverse	5'-TCCCGACGCGGCCGCGGAGTCGTCCAGGTCGTCGTC-3'
RHG125	Forward	5'-CCCTCGGCGCCCATCGGGCCATCGTCCCTGGCTCAGGCCGCGAAC-3'
	Reverse	5'-GTTCGCGGCCTGAGCCAGGGACGATGGCCCGATGGGCGCCGAGGG-3'
RHG126	Forward	5'-GACGACGACCTGGACGACTCGTCCCTGGCTCAGGCC-3'
	Reverse	5'-GGCCTGAGCCAGGGACGAGTCGTCCAGGTCGTCGTC-3'
RHG130	Forward	5'-GCAAACAACAGAGACCCCGGAGCGGGCAGCGACTCCCCCCCGGCC -3'
	Reverse	5'-GGCCGGGGGGGAGTCGCTGCCCGCTCCGGGGTCTCTGTTGTTTGC -3'

For the construction of RHG128 and RHG135, plasmids pHG113 and pHG123 were digested with NruI and MluI. The NruI-MluI fragments that contain the respective deletion of residues 343 to 391 (Δ343–391) and residues 343 to 441 (Δ343–441) were used to replace the wild-type version of the NruI-MluI fragment in plasmid pHG111, which already contains a deletion of ICP0 residues 242 to 291. The resulting plasmids were named

pHG128, which contains double deletions of residues 242 to 291 and residues 343 to 391, and pHG135, which contains double deletions of residues 242 to 291 and residues 343 to 441. For the construction of RHG136, I again adopted the two-round PCR strategy. I used pHG121 as the PCR template and the same primer pair as the one used for RHG114 construction. The product generated from the second-round PCR containing double deletions of residues 242 to 341 and residues 393 to 441 was digested with XhoI and MluI to swap the wild-type XhoI-MluI fragment in pHG101. This resulted in plasmid pHG136. For the construction of RHG137, plasmid pHG130, which contains I362G, V363A, and I364G (I362G/V363A/I364G) mutations, was digested with NruI and MluI. The NruI-MluI fragment containing the I362G/V363A/I364G mutations was used to replace the NruI-MluI fragment in plasmid pHG111, generating an intermediate plasmid pHG111-SLS4m that contains double mutations of Δ242–291 and I362G/V363A/I364G substitutions. We then used the two-round PCR strategy with pHG111-SLS4m as the PCR template and the same primer pair as the one used for RHG114 construction to generate a PCR product containing a triple mutation of Δ242–291 plus Δ393–441 and the I362G/V363A/I364G substitutions. This PCR product was digested with XhoI and MluI to swap the wild type XhoI-MluI fragment in pHG101. This generated plasmid pHG137. The internal deletions and mutations of ICP0 above-described were cloned into the KO5 plasmid (Gu and Roizman, 2009). The series of KO5 constructs were then electroporated into the RR1 strain containing an ICP0-null bacterial artificial chromosome (BAC) (Gu and Roizman, 2009). BAC DNAs extracted from positive colonies were transfected into U2OS cells to generate recombinant viruses. All viruses were plaque purified at least three times on U2OS cells. Viral DNAs were isolated, and the existence of ICP0 mutations in both

terminal and internal repeats was verified by Southern blotting.

Antibodies

The polyclonal anti-PML antibody and monoclonal anti-actin antibody were purchased from Santa Cruz Biotechnology Inc. The monoclonal anti-mCherry antibody was purchased from Clontech. The polyclonal anti-USP7 antibody was purchased from Bethyl Laboratories Inc.

Confocal microscopy

HEL cells were seeded on four-well glass slides (Thermo Fisher Scientific) one day before infection. At indicated time points after infection, cells were fixed in 4% paraformaldehyde, permeabilized with 0.2% Triton X-100, and blocked with phosphate-buffered saline (PBS) containing 5% horse serum plus1% bovine serum albumin. The cells were then reacted with indicated primary antibodies at 4°C overnight, rinsed, and reacted with fluorescein isothiocyanate (FITC)-conjugated goat anti-rabbit (Sigma) plus Texas Red-conjugated goat anti-mouse (Invitrogen) secondary antibodies. Images were taken with a Zeiss LSM780 confocal microscope at the Microscopy, Imaging & Cytometry Resources (MICR) Core Facility at Wayne State University School of Medicine. Three-dimensional (3D) images were constructed through Volocity 3D image analysis software.

Coimmunoprecipitation

HEp-2 cells were seeded into 100mm dishes one day before infection with the test viruses at 5 pfu/cell. After overnight infection, the cells were harvested and lysed in lysis buffer (10 mM Tris-HCl [pH 8.0], 140 mM NaCl, 1.5 mM $MgCl_2$, 1 mM dithiothreitol, and 0.5% NP-40 supplemented with a protease inhibitor cocktail [Sigma] and a phosphatase inhibitor cocktail [Sigma]). After brief sonication and centrifugation to remove the cell

debris, the total cell lysates were precleared by incubation with 50% slurry of protein A-Sepharose CL-4B beads (GE Healthcare, Pittsburgh, PA) at 4°C for 20 min. Upon beads removal, the cleared lysates were incubated with a rabbit polyclonal antibody to USP7 overnight at 4°C. The lysate-antibody mixtures were then incubated with 50% slurry of protein A-Sepharose CL-4B beads at 4°C for 2 h. The beads were then rinsed four times with lysis buffer and eluted with 1× Laemmli buffer at 95°C for 5 min. The elutes were electrophoretically separated on 8% sodium dodecyl sulfate-polyacrylamide gel electrophoresis (SDS-PAGE) gels and subjected to Western blot analysis.

Western blot analysis

HEL or HEp2 cells were mock infected or infected with 10 pfu/cell of recombinant viruses for 1 h. The inocula were then removed, and cells were incubated in DMEM supplemented with 10% newborn calf serum (Thermo Fisher Scientific). At 8 hpi, the cells were harvested, washed, and lysed in radioimmunoprecipitation assay (RIPA) buffer (50 mM Tris [pH 7.4], 150 mM NaCl, 1 mM EDTA, 0.1% SDS, 1% NP-40, 0.25% sodium deoxycholate, 1 mM phenylmethylsulfonyl fluoride). The total cell lysates were sonicated, electrophoretically separated on SDS-PAGE gels, and then transferred onto a polyvinylidene difluoride (PVDF) membrane (Millipore). The membrane was blocked with 1×Tris-buffered saline–Tween (TBST) (20 mM Tris [pH 7.5], 150 mM NaCl, 0.5% Tween 20) containing 5% nonfat dry milk and probed with indicated primary antibodies. The membrane was then incubated with horseradish peroxidase-conjugated goat anti-mouse or goat anti-rabbit secondary antibody (Sigma) and visualized with ECL Western blotting detection reagent (GE Healthcare).

Results

Deletion of continuous 50, 100, and 150 amino acids within ND10-ES does not reveal a specific region required for ND10 fusion

Previously, our lab has reported that the dynamic interaction between ICP0 and ND10 is composed of three sequential steps: adhesion, fusion, and retention (Gu et al., 2013). We have identified the central region of ICP0, which contains residues 245 to 474, as ND10 entry sequence (ND10-ES). When ND10-ES is deleted, the ND10 fusion process is blocked after adhesion, and ICP0 juxtaposes with ND10 for a short period (Gu et al., 2013).

My first project was to identify the minimum sequences necessary for ND10 fusion, I conducted deletion mapping of the ICP0 central region and examined positions of ICP0 mutants relative to those of ND10 nuclear bodies through high-resolution immunofluorescence confocal imaging. Throughout the study, PML, the ND10 organizer, was immunostained to represent the ND10 distribution in the nucleus. Recombinant virus RHG110 (Fig 2.1A, line 2), which lacks ND10-ES in ICP0, was used as the control for ICP0-ND10 juxtaposition (Fig 2.2B, panels a to d). Recombinant virus RHG120 (Fig 2.1A, line 2) containing C116G/C156A substitutions in ICP0 RING domain (RING finger mutant [RFm]), in which ICP0 is incapable of degrading PML (Gu and Roizman, 2009) and sequestered within ND10 throughout the infection, was used as a control for ICP0-ND10 colocalization (Fig 2.2A, panels a to d). The reason I chose ICP0 RFm (RHG120) as a control for ICP0-ND10 colocalization instead of wild-type ICP0 was to prevent PML degradation and avoid the disappearance of the PML signal (ND10 marker) during infection. For each ICP0 mutant constructed in this study (Fig 2.1B, panels 1 to 4), subnuclear distributions of ICP0 mutants were examined and compared with both the
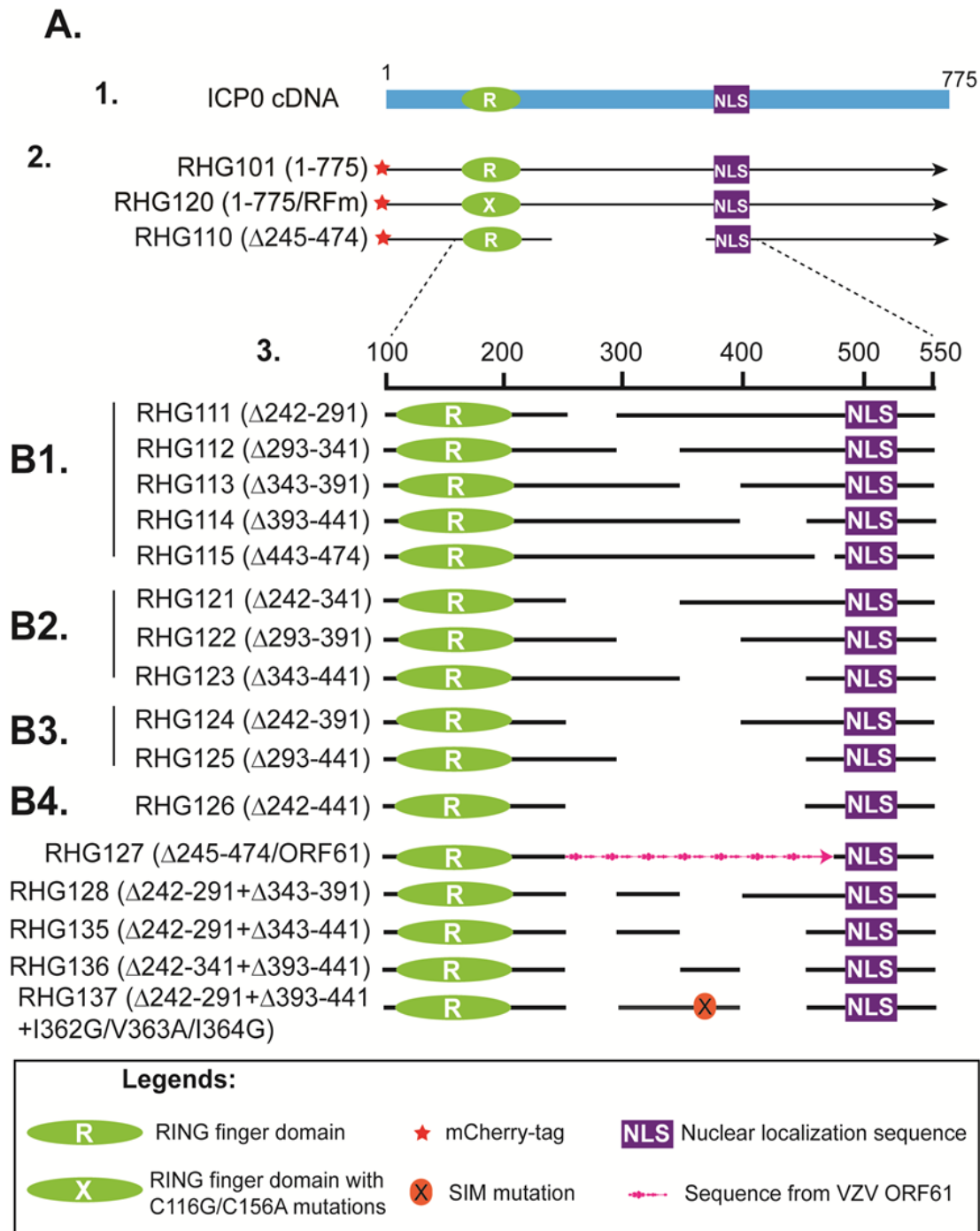
Fig 2.1: Schematic diagrams of ICP0 mutants used in Chapter 2. (A) Line 1 shows ICP0 cDNA (775 amino acids) used for mutant construction, with positions of the RING finger domain and nuclear localization sequence shown. Line 2 shows schematic diagrams of recombinant viruses RHG101, RHG120, and RHG110 (Gu et al., 2013). Line 3 shows amino acid positions in the expanded region of residues 100 to 550. (B1 to B4) Recombinant viruses containing deletions and mutations in ICP0. The amino acid deletions and mutations are indicated in parentheses following the virus names. Symbols representing specific domains are shown in the key.

ND10 juxtaposition control (RHG110) and the ND10 colocalization (fusion) control (RHG120) to determine the relative positions of mutant ICP0 and ND10. ICP0 mutants which juxtaposed with ND10 are defined as ND10 fusion-incompetent, while those that colocalized with ND10 are defined as ND10 fusion-competent.
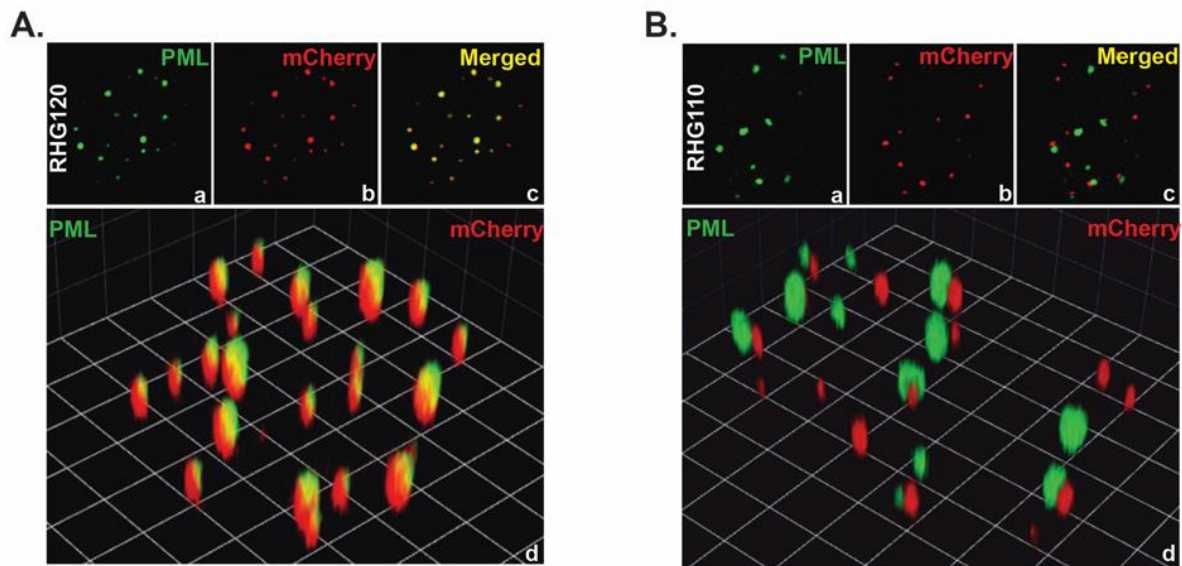
Fig 2.2: ICP0 localization of recombinant viruses RHG120 and RHG110. HEL cells were infected with RHG120 (A), RHG110 (B) at 10 pfu/cell. At 3 hpi, cells were fixed, permeabilized, and reacted with polyclonal anti-PML and monoclonal anti-mCherry antibodies. Two- and three-dimensional images of representative infected cells were taken with a Zeiss LSM780 confocal microscope. The three-dimensional images were reconstructed with Volocity software.

When I started working on this project, a few recombinant HSV-1 viruses had been constructed to map the minimum sequences for ND10 fusion. Recombinant viruses RHG111 to RHG115, in which ICP0 carry 50 amino acids deletions, were first constructed. These deletions covered the full length of ND10-ES. All of them showed colocalization with ND10 (Zheng and Gu, 2015). Then RHG121 to RHG123, RHG124, and RHG125, in which ICP0 was deleted of 100 and 150 amino acids within ND10-ES were constructed to encompass the entire area of residues 242 to 441 (Fig 2.1B, panels

1 to 3). All ICP0 mutants with a deletion of 100 or 150 amino acids showed colocalization with ND10 (Fig 2.3), suggesting that continuous removal of 50, 100, and 150 amino acids do not affect ICP0 to fuse with ND10.
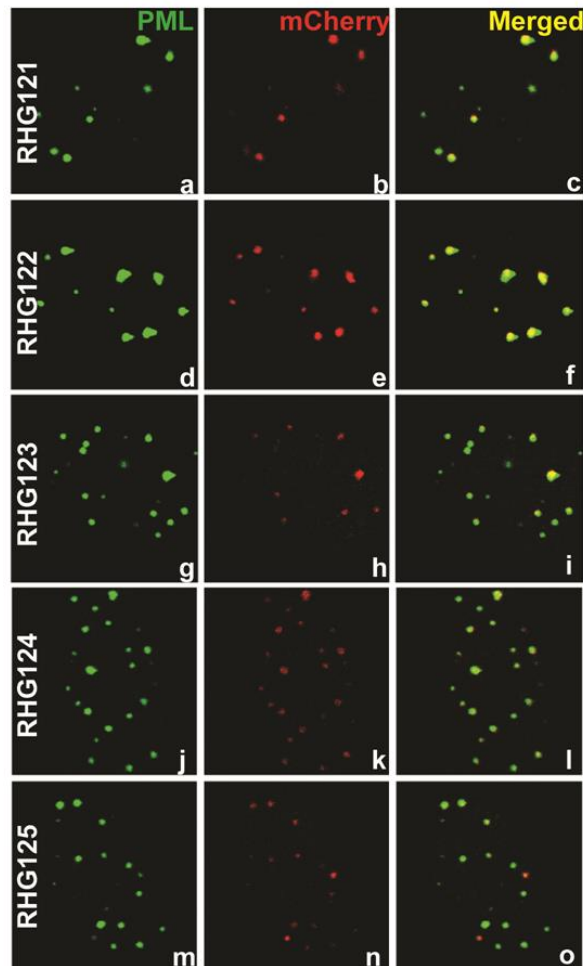
Fig 2.3: ICP0 localization in recombinant viruses containing a 100- or 150-amino acids deletion in the central region of ICP0. HEL cells were infected with the indicated recombinant viruses at 10 pfu/cell. At 3 hpi, cells were processed and stained as described above. Representative images of infected cells were taken with a Zeiss LSM780 confocal microscope.

Functional ND10-ES encompasses 200 amino acids

Since deletion of 50, 100, or 150 amino acids did not illustrate any region essential for ND10 fusion, I constructed recombinant virus RHG126 (Fig 2.1B, panel 4), in which ICP0 contains a deletion of 200 amino acids between residues 242 and 441. ICP0 without

amino acids 242 to 441 juxtaposed with ND10, unable to fuse with ND10 (Fig 2.4, panels a to d) similar to ND10 juxtaposition control RHG110. Recapitulation of ND10 juxtaposition from independently constructed virus RHG126 ruled out the possibility that mutant ICP0 juxtaposition with ND10 was just incidental mutations in other viral genes instead of ICP0. The reproducibility between RHG110 and RHG126 emphasized the significance of the ICP0 central region in ND10 fusion. These results indicate that residues 242 to 441 encompassing 200 amino acids within ND10-ES are essential for ND10 fusion and smaller continuous deletions fail to disrupt ND10 fusion.
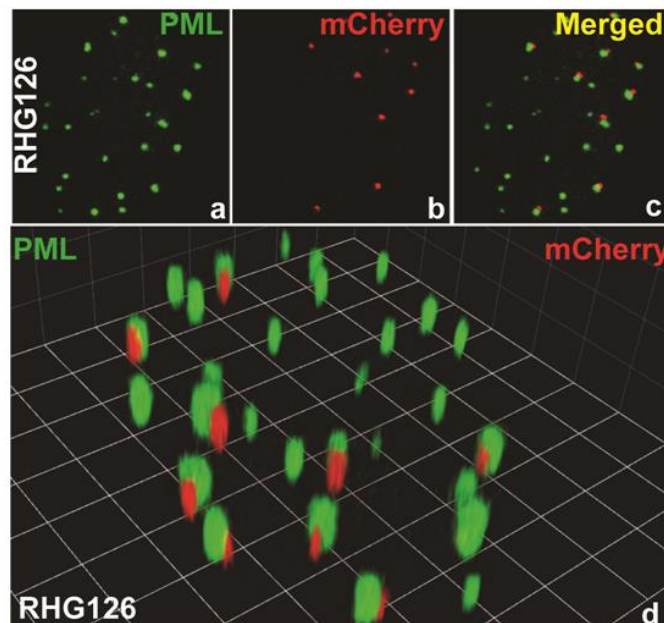
Fig 2.4: ICP0 localization of recombinant virus RHG126. HEL cells were infected with RHG126 at 10 pfu/cell. At 3 hpi, cells were processed and stained above.

Replacement of ND10-ES by the corresponding region from VZV ORF61 does not recover ND10 fusion

Two possible scenarios can explain why the minimum ND10 fusion sequence cannot be narrowed down to less than 200 amino acid sequences. First, residues 242 to 441 of

ICP0 constitute a flexible linker region between the N and C termini of ICP0. The particular length of this region, instead of sequence specificity, is essential for maintaining the overall structure of ICP0 and supporting the fusion of ICP0 with ND10. Second, multiple and discontinuous segments within residues 242 to 441 redundantly facilitate ICP0 fusion with ND10. The previous deletions of 50, 100, or 150 amino acids only disrupt a fraction of the redundant elements, while remaining elements are still active to drive ND10 fusion.
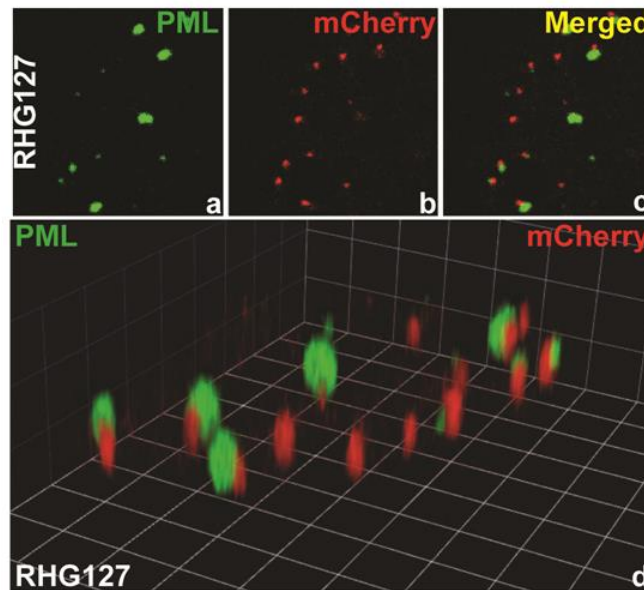
Fig 2.5: ICP0 localization of recombinant virus RHG127. HEL cells were infected with RHG127 at 10 pfu/cell. At 3 hpi, cells were processed and stained as described above.

To test the first scenario, I constructed recombinant virus RHG127 (Fig 2.1B, panel 4), in which the corresponding region of ORF61 (amino acids 105 to 335) from VZV replaces residues 245 to 474 of ICP0. The results showed that chimerical ICP0 was unable to fuse with ND10 and showed juxtaposition with ND10 nuclear bodies (Fig 2.5, panels a to d), similar to ICP0 with deletion of ND10-ES in RHG110-infected cells (Fig 2.2B, panels a to d). Reconstitution of the distance between the N and C termini of ICP0 did not recover

ND10 fusion, suggesting the particular sequences not the length of the ICP0 central region is responsible for ND10 fusion.

Deletion of the ND10-ES in ICP0 does not affect its interaction with USP7 but affects its E3 ubiquitin ligase activity

To further exclude the possibility that ND10 juxtaposition is the result of protein aggregation caused by structural change, I evaluated the effects of internal deletion on the overall functions of ICP0.

I first assessed the activity of ICP0 functional domain for interaction with USP7. The USP7 binding activity is located within C-terminal residues 594 to 633 (Meredith et al., 1995). To check whether the ND10-ES deletion or the insertion of VZV ORF61 corresponding region can change ICP0 overall structure, I performed a Co-IP assay to examine the USP7 binding ability of ICP0. Full-length ICP0 from virus RHG101 was used as the positive control for USP7 binding, and C-terminally truncated ICP0 from virus RHG104 (Gu et al., 2013), in which the USP7 binding region is deleted, was used as the negative control. As expected, USP7 efficiently pulled down full-length ICP0 from infected cells (lane 5 in Fig 2.6A, panel a), while it did not bind with ICP0 with C-terminal truncation (lane 6 in Fig 2.6A, panel a). ICP0 mutants from both internal truncation (RHG110) and VZV replacement (RHG127) were capable of binding with USP7 (lanes 7 and 8 in Fig 2.6A, panel a), suggesting that neither the internal truncation nor the sequence replacement from ORF61 affects the overall structure, especially the C-terminus of ICP0.

Besides evaluating the effect of internal deletion on the C-terminal functional domain of ICP0, I also examined the E3 ubiquitin ligase activity located in the ICP0 N-terminus. Previously, our lab reported that the degradation of PML was abolished for the internally

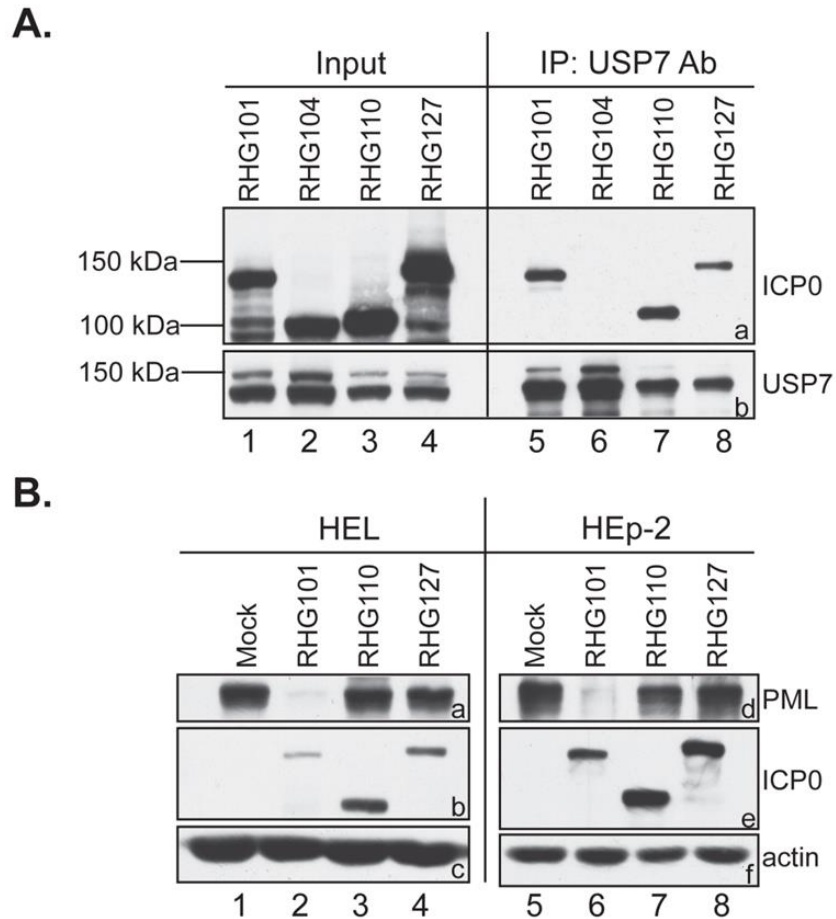truncated ICP0 of RHG110 (Gu et al., 2013). In this experiment, both RHG110 and

Fig 2.6: Deletion of the ND10-ES in ICP0 does not affect its interaction with USP7 but affects its E3 ubiquitin ligase activity. (A) ICP0 internal deletion or insertion does not affect its interaction with USP7. HEp2 cells were infected with indicated recombinant viruses at 5 pfu/cell for 14 h. Lysates from infected cells were then subjected to a coimmunoprecipitation (IP) assay with a polyclonal anti-USP7 antibody. The immunoprecipitates were electrophoretically separated on SDS-PAGE gels and probed with the indicated antibodies. (B) ICP0 internal deletion reduces its E3 ligase activity in PML degradation. HEL and HEp-2 cells were mock-infected or infected with recombinant viruses RHG101, RHG110, and RHG127 at 10 pfu/cell. At 8 hpi, total cell lysates were probed with the indicated antibodies through Western blotting.

RHG127 were not able to degrade PML in HEL (lanes 3 and 4 in Fig 2.6B, panel a) and

HEp-2 cells (lanes 7 and 8 in Fig 2.6B, panel d). These results indicate that ND10-ES

deletion or VZV replacement affects ICP0 E3 ligase activity to degrade PML. Various

reports have shown that the E3 ligase activity of ICP0 is regulated by multiple factors including CoREST binding (Gu and Roizman, 2009) and SUMO interaction motif (Boutell et al., 2011). Even though we cannot rule out the possibility that deletion of ND10-ES affects the RING structure, it is safe to propose that even without structural changes in the RING, deletion of the ICP0 central region can have significant impacts on the E3 ligase activity of ICP0.

Simultaneous deletions of residues 242-291 and 343-441 abolish ND10 fusion

To test the possibility that multiple segments redundantly drive ICP0 to fuse with ND10, I constructed another two recombinant viruses, namely RHG135 and RHG136 (Fig 2.1B, panel 4), in which a sum of 150 amino acids is deleted in a discontinuous manner. Then I examined the localization of these two mutant ICP0s. As shown in Fig 2.7A, representative RHG135 was unable to fuse with ND10, showing juxtaposition with ND10. In contrast to RHG135, ICP0 of RHG136 could fuse with ND10 (Fig 2.7B, panels a to d).

I then tabulated the number of RHG135 and RHG136 infected cells containing discrete dotted structures. At 1.5 hpi, within 200 cells tabulated, 47% of cells infected with RHG110, 50% of cells infected with RHG135, and 42% of cells infected with RHG136 expressed ICP0 to a detectable level (Fig 2.7C). The similar percentage of infected cells indicated that levels of the initial viral loads were comparable for the control and experiment viruses (Fig 2.7C).

Our lab previously reported that ICP0 lacking ND10-ES (RHG110) transiently juxtaposed with ND10. Only about one-third of the RHG110-infected cells contain punctate ICP0 structures at 1.5 hpi, and this number decreased as infection progressed (Gu et al., 2013). As shown in Fig 2.7D, reproducible results for RHG110 were again
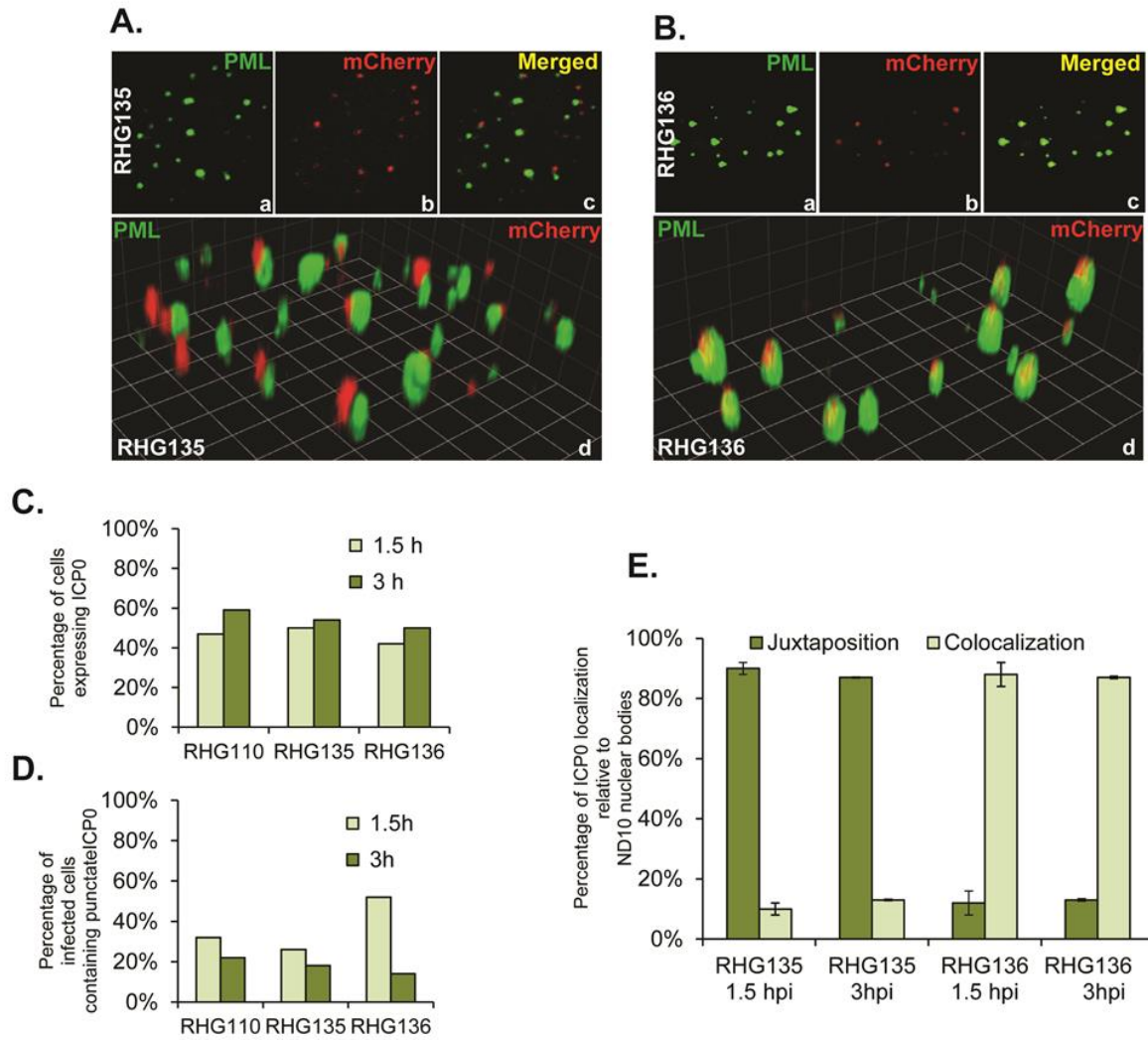
Fig 2.7: Simultaneous deletions of residues 242 to 291 and residues 343 to 441 in the central region of ICP0 abolish ND10 fusion. (A and B) HEL cells were infected with RHG135 (A) and RHG136 (B) at 10 pfu/cell. At 1.5 hpi, infected cells were fixed, stained, and visualized as described above. (C and D) At 1.5 and 3 hpi, cells expressing ICP0 (C) and containing ICP0 exclusively in punctate structures (D) were tabulated. (E) At 1.5 and 3 hpi, relative positions of ICP0 and ND10 dots (juxtaposition or colocalization) were tabulated.

observed. A similar pattern of ICP0 distribution was found in RHG135 infection (Fig 2.7D).

Compared with cells infected by RHG135, more RHG136-infected cells had punctate

ICP0 structures at 1.5 hpi, and this number dropped faster from 1.5 hpi to 3 hpi (Fig 2.7D).

I further examined the positions of dotted ICP0 relative to that of ND10 with high

magnification (100x) objectives. I tabulated ICP0 and ND10 dots in two groups of 20 infected cells that contained ICP0 exclusively in punctate dots with no detectable nucleoplasmic staining. On average, 15 to 20 ND10 bodies exist per HEL cell. I further examined 300 to 400 nuclear dots stained by PML antibody for each 20-cell group. In cells infected by RHG135, at 1.5 and 3 hpi, averages of 89.2% and 85.6% of the ICP0 dots juxtaposed with ND10, while 9.7% and 13.2% of the ICP0 dots colocalized with ND10, respectively (Fig 2.7E). Opposite to cells infected by RHG135, averages of 11.9% and 12.6% of the RHG136 ICP0 dots juxtaposed with ND10 at 1.5 and 3 hpi, while 87.8% and 86.5% of the ICP0 dots colocalized with ND10, respectively (Fig 2.7E). In both RHG135 and RHG136 infections, 1% of the ICP0 dots aggregated without an apparent association with ND10. These results indicate simultaneous deletions of bipartite regions including residues 242 to 291 and residues 343 to 441 cause ICP0 to juxtapose at the ND10 surface but fail to fuse with the ND10 bodies.

Three redundant segments within residues 242 to 441 independently promote the fusion of ICP0 with ND10

To analyze ICP0 sequences involved in ND10 fusion, I compiled the ND10 fusion results from all recombinant viruses.

First, I compared ICP0 from RHG125, which is ND10 fusion competent (Fig 2.1B, panel 3), with ICP0 from RHG126, which is ND10 fusion incompetent (Fig 2.1B, panel 4). The additional residues 242 to 291 (RHG125) caused ICP0 from juxtaposing to fusing with ND10, indicating that the sequences between residues 242 and 291 are enough to drive ND10 fusion and defined as ND10 fusion segment 1 (ND10-FS1).

Both ICP0 mutants from RHG135 and ICP0 from RHG126 juxtaposed with ND10 and

failed to fuse with ND10, suggesting that additional residues 292 to 341 (RHG135) are not involved in the ND10 fusion process.

Next, I compared ICP0 from RHG136, which is ND10 fusion competent (Fig 2.1B, panel 4), with ICP0 from RHG126 (Fig 2.1B, panel 4). An additional insertion of residues 343 to 391 (RHG136) changed ICP0 from juxtaposition to fusion with ND10. Therefore, residues 343 to 391 are sufficient to facilitate ND10 fusion and defined as ND10 fusion segment 2 (ND10-FS2).

Lastly, I compared ICP0 from RHG124, which is ND10 fusion competent (Fig 2.1B, panel 3), with ICP0 from RHG126 (Fig 2.1B, panel 4). Again, the additional residues 393 to 441 (RHG124) recovered ICP0 from ND10 juxtaposition to fusion, implying that the residues 393 to 441 contain another segment sufficient for ICP0 to fuse with ND10. To confirm residues 393 to 441 are another ND10 fusion segment, I constructed another recombinant virus, RHG128 (Fig 2.1B, panel 4), in which ICP0 central region contains residues 292 to 341 and residues 393 to 441. As aforementioned, residues 292 to 341 are not supportive of ND10 fusion. Therefore, the ND10 fusion competency of RHG128 solely depends on residues 343 to 441. The vast majority of ICP0 showed colocalization with ND10 in RHG128-infected cells (Fig 2.8). Statistical analysis indicated that 95.0% of the ICP0 (RHG128) dots colocalized with ND10, while around 4% of the ICP0 dots juxtaposed with ND10. Comparing RHG128 with RHG135, the additional residues 393 to 441 caused ICP0 localization to change from juxtaposition to fusion. Results from both the RHG124/RHG126 comparison and the RHG128/RHG135 comparison led to the same conclusion that residues 393 to 441 of ICP0 are also enough to facilitate ICP0 ND10 fusion and defined as the third fusion segment (ND10-FS3).
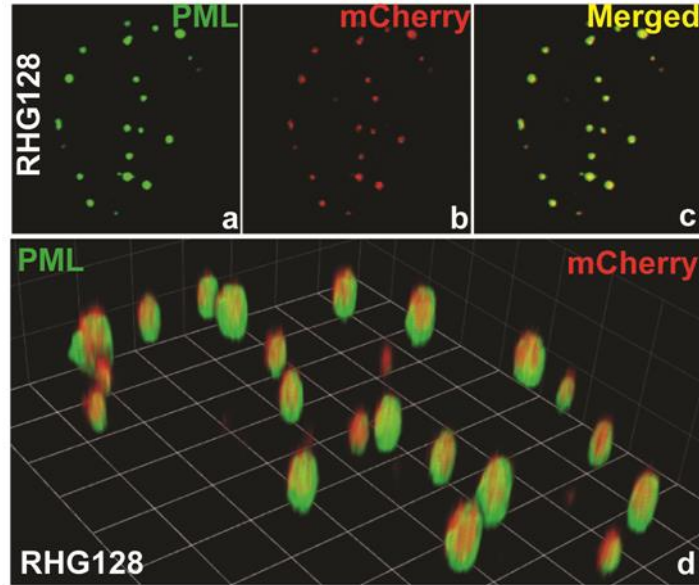
Fig 2.8: ICP0 localization of recombinant virus RHG128. HEL cells were infected with RHG128 at 10 pfu/cell. At 3 hpi, cells were processed and stained as described above.

SUMO Interaction Motif-like Sequence 4 (SLS4) located within ND10-FS2 is not essential for ND10 fusion

Boutell et al. reported seven SLSs scattering throughout ICP0 (Boutell et al., 2011) that may regulate ICP0 degradation of SUMO-modified substrates. Among them, SLS4 has been shown to interact with SUMO2/3 and promote ubiquitination through *in vitro* polyubiquitination assays (Boutell et al., 2011). SLS4 (I362, V363, and I364) resides within ND10-FS2 (residues 343 to 391). To examine whether SLS4 plays any role in the ND10 fusion, I constructed a recombinant virus in which ND10-FS1 and ND10-FS3 are deleted, but ND10-FS2 is retained with point mutations I362G, V363A, and I364G (Fig 2.1B, panel 4). The result showed that the majority of ICP0 in RHG137-infected cells fused with ND10 (Fig 2.9A, panels a to d). Statistical results showed more than 60% of the mutant ICP0 dots from RHG137 infected cells colocalized with ND10 (Fig 2.9B),

suggesting that SLS4 is not essential for ND10 fusion but may play an auxiliary role in facilitating an efficient fusion.
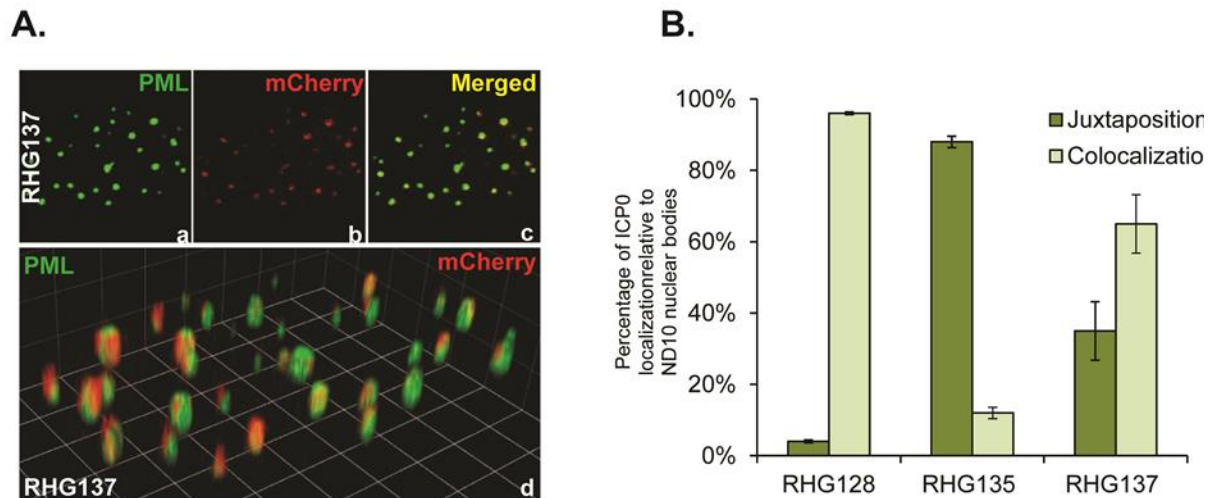

Fig 2.9: ICP0 localization of recombinant virus RHG137. (A) HEL cells were infected with RHG137 at 10 pfu/cell. At 3 hpi, cells were processed and stained as described above. (B) At 1.5 hpi, relative positions of ICP0 and ND10 dots (juxtaposition or colocalization) were tabulated.

Discussion

Since PML and other components of ND10 have been implicated in mediating both intrinsic and innate immunity, many DNA viruses modify or disrupt ND10 as a counteraction to enhance viral replication (Tavalai and Stamminger, 2008). In HSV-1, ICP0 colocalizes with ND10 and degrades PML and Sp100 to dampen the repressions imposed by ND10 (Everett et al., 2006). Our lab has reported the interaction between ICP0 and ND10 includes three sequential steps: adhesion, fusion, and retention (Gu et al., 2013). In each step, ICP0 likely interacts with different sets of ND10 components to degrade the restrictive factors or capture the beneficial constituents, both of which are essential for efficient viral replication. ND10 fusion is the phase in which ICP0 has access to ND10 components. Therefore, it is likely a particularly critical stage for ICP0 to execute

its function.

In this study, I focused on identifying the minimum sequences for ND10-ES essential for ND10 fusion. Through deletion mapping and confocal imaging to examine the localization of ICP0 mutants, I identified three redundant sequences which independently drive ND10 fusion. A natural question is whether these three segments drive ND10 fusion to a similar extent. According to our results, there is no significant difference in driving efficiency for these three sequences at a 10 pfu/cell for 1.5 hpi. With current technology, it is difficult to resolve whether these three segments expedite the fusion process at a comparable level at low MOI infection. The speed of ND10 fusion possibly can be compared through live imaging to observe the ND10 fusion by each mutant ICP0 containing only one ND10 fusion segment. Another question is why ICP0 needs to have redundant elements for ND10 fusion, which seems contradictory to the viral coding economy. The existence of redundant ND10 fusion elements may reflect the significance of this step during HSV-1 infection. These redundant and cooperative interactions may also be the reason why ND10 fusion occurs at a massive speed.

The three ND10 fusion segments share 9.4% identity positions and 52.8% consensus positions through sequence alignment of the Vector NTI program (Fig 2.9A). A conserved feature of all three segments is the high proline percentage (Fig 2.9B). Proline residues constitute an average of 28% of the total of 150 amino acids in the three ND10-FSs, whereas the overall proline content for ICP0 is 13%. Residues 292 to 341 of ICP0 and residues 105 to 335 of ORF61, both of which cannot support ND10 fusion, are composed of 6% and 11% proline, respectively. All these observations suggest a correlation between proline-rich sequences and ND10 fusion.
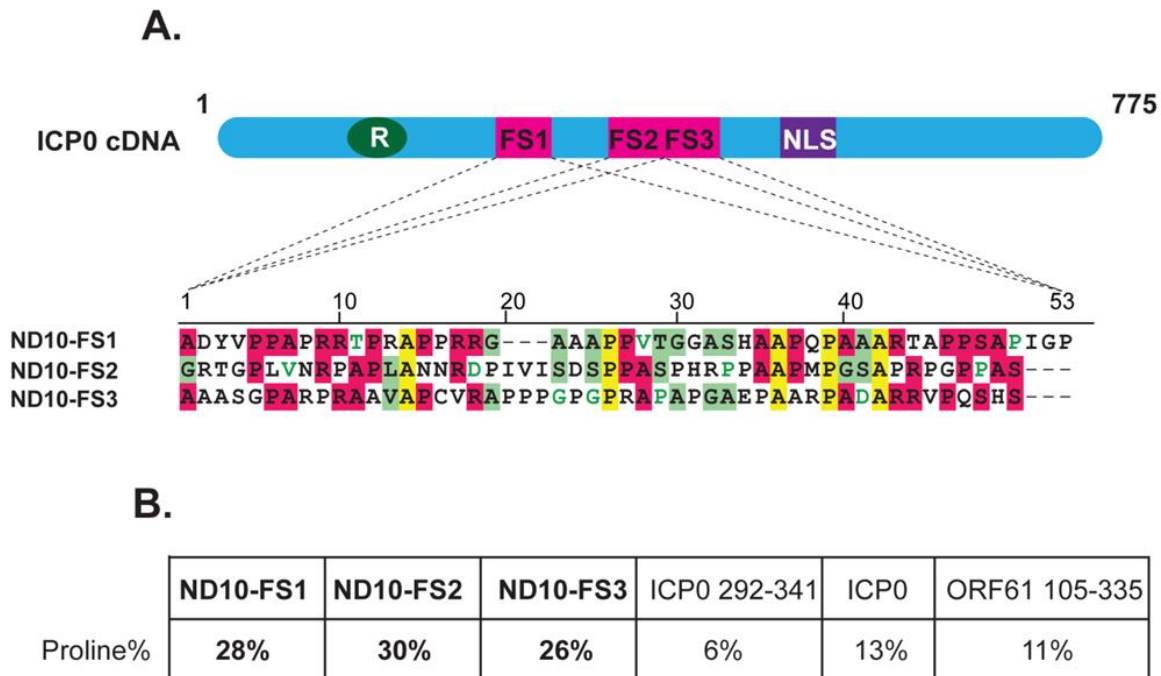
Fig 2.10: Redundant ND10 fusion segments are proline-rich elements. (A) Alignment of the three ND10-FS sequences. The positions of ND10-FS1, ND10-FS2, and ND10-FS3 in ICP0 cDNA are illustrated. Sequence alignment was conducted by using sequence alignment program of Vector NTI software. In the aligned sequences, identical amino acids are highlighted in yellow, conservative amino acids are highlighted in red, amino acids with high similarity are highlighted in green, and amino acids with weak similarity are illustrated by light green letters. (B) Calculation of proline percentage in ND10 fusion segments, ICP0 residues 292-341, full-length ICP0 and VZV ORF61 residues 105-335. The proline-rich ND10-FS segments and their proline percentages are highlighted in bold.

Proline-rich sequences have the propensity to form a polyproline-II (PPII) helix, a secondary structure less abundant than the α helix and β sheet (Adzhubei et al., 2013). Due to the cyclic side chains of proline residues, PPII helix has an open and relatively extended structure (Rath et al., 2005). Besides, PPII helix tends to be located on the surface of a folded protein and is more flexible than α helix and β sheet due to the absence of inter- and intra-hydrogen bonds (Adzhubei et al., 2013). These structural features make PPII helix highly suitable for mediating protein-protein and protein-nucleic acids

interactions. The known modules which interact with PPII helix include the SH3 domain, the WW domain, and the Enabled/VASP homology 1 (EVH1) domain (Rath et al., 2005). The protein-protein interaction mediated by PPII helix bears less specificity and higher flexibility when interacting with its binding partners (Siligardi and Drake, 1995). This attribute of PPII helix supports ICP0 transient interactions with dynamic components of ND10. In the future, we will investigate the structure of ND10 fusion segments and the correlation between structure and function of these ND10 fusion segments.

CHAPTER 3 IDENTIFICATION OF ELEMENTS REGULATING A DIFFERENTIAL SUBSTRATE RECOGNITION BY THE ICP0 E3 UBIQUITIN LIGASE OF HSV-1

Part of this work has been published in:

Introduction

ICP0 of HSV-1 is an immediate early viral protein which is essential for lytic infection in low multiplicity of infection. The major role of ICP0 in HSV-1 infection is to counteract host intrinsic and innate antiviral immunity. Sensing viral entry, one immediate early event in the host cell is the convergence of nuclear domain 10 (ND10) with viral DNA to repress viral expression. ICP0, with RING-dependent E3 ubiquitin ligase, causes the proteasome-dependent degradation of PML and Sp100, two major components of ND10, and disperses other inhibitory ND10 components to alleviate repression (Chelbi-Alix and de The, 1999; Maul et al., 1993).

In addition to PML and Sp100, ICP0 also utilizes its E3 ligase activity to target other substrates, such as RNF8, DNA-PKcs, IFI16, centromere proteins (CENPs) (Gu, 2016). ICP0 has been reported to possess multiple mechanisms to ubiquitinate and degrade different E3 substrates (Boutell and Everett, 2013). First, direct interaction with USP7 leads to the reduction of USP7. Second, phosphorylation of ICP0 residue T67 mediates the interaction with FHA domain of RNF8 and is responsible for RNF8 degradation. Third, ICP0 is a SUMO-targeted ubiquitin ligase (STUBL) and uses its SUMO Interaction Motif (SIM) to target SUMOylated proteins for degradation, such as SUMOylated PML. Knockdown of ICP0 substrates mentioned above can increase viral expression and

replication to different extents, indicating that these proteins are part of the antiviral defense (Gu, 2016). These substrates are involved in multiple cellular pathways, including interferon response, DNA damage response, chromatin remodeling, suggesting that ICP0 manipulates and counteracts multiple cellular pathways for efficient viral gene expression. However, the molecular basis for regulation of the differential substrate recognition and degradation remains unclear. To understand ICP0 coordination of its domains in recognizing different E3 substrates from a diverse array of cellular pathways, I took the approach to dissect the functional domains that are responsible for ICP0 to differentiate its sample substrates, PML isoforms.

In this chapter, I focus on identifying elements in ICP0 that regulate its E3 ligase activity, specifically sequences regulating recognition and degradation of PML isoforms. Through deletion mapping and half-life assay, at least two distinct mechanisms have been found to be responsible for differential degradation of PML isoforms. I also tested the relationship between ND10 fusion and PML degradation since ND10 fusion process presumably helps ICP0 to approach its substrates located within ND10. Moreover, I also evaluated the biological significance of the domain that mediates ICP0 substrate recognition.

Material and Methods

Cells

HEL and HEp-2 cells were cultured as described in Chapter 2. HEp-2-TetOn cells were grown in DMEM medium (Invitrogen) supplemented with 10% FBS and 6 µg/ml blasticidin (Invitrogen).

Construction of HEp-2-TetOn expressing MycPML I or MycPML II cells

Dr. Haidong Gu constructed the parental HEp-2-TetOn cell (Zheng et al., 2016). Based on HEp-2-TetOn cell, Drs. Subodh Samrat and Haidong Gu built the subsequent HEp-2-TetOn expressing MycPML I or MycPML II cell, respectively.

Viruses

Recombinant viruses RHG101, 103, 104, 105, 110, 118, and 120 were constructed by Dr. Haidong Gu and had been described elsewhere (Gu et al., 2013). Construction of the other viruses used in this study has been described in Chapter 2.

Antibodies

The polyclonal anti-PML antibody, monoclonal anti-actin antibody, and monoclonal anti-Myc antibody were purchased from Santa Cruz Biotechnology Inc. The polyclonal anti-mCherry antibody was purchased from Clontech. The polyclonal anti-Sp100 antibody and monoclonal anti-ubiquitin antibody were purchased from Abcam.

Western blot

HEL, HEp-2, or HEp-2-TetOn expressing MycPML isoforms cells were mock infected or infected with 10 pfu/cell of indicated recombinant viruses for 1 h. Inocula were then removed, and cells were incubated in DMEM supplied with 10% newborn calf serum. At the hours indicated, the cells were harvested, washed, and lysed in RIPA buffer. The total cell lysates were sonicated, electrophoretically separated on SDS-PAGE, and then transferred to PVDF membrane. The membrane was blocked and probed with indicated primary antibodies. The membrane was then incubated with horseradish peroxidase-conjugated goat anti-mouse or goat anti-rabbit secondary antibody and visualized with ECL Western Blotting Detection Reagent.

Half-life assay

HEp-2-TetOn cells expressing MycPML isoforms were induced with 1 µg/ml doxycycline (Dox) overnight and then exposed to a test virus at 10 pfu/cell for 1 h. The inoculum was removed, and the cells were incubated in growth medium for 1 h before 100 µg/ml cycloheximide (CHX) was added. Cells were harvested at 2-h intervals until 6 h post-treatment of CHX. The total cell lysates were subjected to Western blotting. Bands of PML isoforms were scanned and quantitated with ImageJ software.

Confocal microscopy

HEp-2-TetOn cells expressing MycPML I or MycPML II seeded on four-well glass slides were induced with 1 µg/ml Dox for 24 h. Then cells were fixed, permeabilized, and blocked as described in Chapter 2. The cells were then reacted with rabbit anti-Sp100 and mouse anti-Myc antibodies at 4°C overnight, rinsed, and reacted with fluorescein isothiocyanate-conjugated goat anti-rabbit and Texas Red-conjugated goat anti-mouse secondary antibodies. Images were taken with a Leica SP8 confocal microscope.

qPCR

HEp-2-TetOn cells expressing MycPML II grown on 35-mm plates were induced with 1 µg/ml Dox overnight before being infected with a test virus at 0.1 pfu/cell for 1 h. The inoculum was then removed, and cells were incubated in DMEM supplemented with 10% newborn calf serum. At 2 and 24 hpi, total DNA was extracted through phenol-chloroform method. Quantitative PCR (qPCR) was performed using Absolute qPCR SYBR Green ROX mix (Thermo Fisher Scientific) and a QuantStudio 3 Real-Time PCR Systems (Thermo Fisher Scientific). Primers 5′-GCAGCTAGCATGGCGACTGACATTGATATG-3′ and 5′-GCAGAATTCCTAAAACAGG GAGTTGCAATA-3′ targeting the α27 (ICP27) gene were used for viral DNA quantitation. The QuantumRNA Universal 18S internal standard

was used as an endogenous control to normalize the DNA amount. The DNA fold increase from 2 hpi to 24 hpi was calculated by comparative $\Delta\Delta C_T$ analysis.

qRT-PCR

HEp-2-TetOn cells expressing MycPML I or MycPML II grown on 35-mm plates were induced with 1 µg/ml Dox overnight before being infected with a test virus at 10 pfu/cell for 1 h. The inoculum was then removed, and cells were incubated in DMEM supplemented with 10% newborn calf serum. At times indicated, total RNA was extracted, and cDNA was synthesized with the SuperScript III First-Strand Synthesis System (Thermo Fisher Scientific). Quantitative RT-PCR was performed with primers 5′-ATGGCATCAATGCAGAAGCTGATCT-3′ and 5′-CTGGAACTCCTCCTCCGAAG-3′ to detect MycPML isoforms. 18S rRNA primers (Ambion) were used for normalization.

PML I *in vivo* ubiquitination assay

HEp-2-TetOn cells expressing MycPML I were induced with 1 µg/ml Dox for 24 h before being exposed to a test virus with 10 pfu/cell. At 2 hpi, cells are scraped, washed and lysed in urea lysis buffer (8 M urea, 100 mM Na_2HPO_4/ NaH_2PO_4 [pH 8.0], 10 mM Tris-HCl [pH 8.0], 5 mM imidazole). Then the cell lysates were subject to brief sonication before spinning down at 14000 rpm for 5 min. The supernatant was incubated with nickel beads (Eppendorf) for 4 h at room temperature with gentle agitation. After incubation, the beads were washed four times. First time with urea lysis buffer; the second time with urea wash buffer (8 M urea, 100 mM Na_2HPO_4/ NaH_2PO_4, 10 mM Tris-HCl [pH 6.8], 5 mM imidazole, 10mM β-mercaptoethonal); and the third time with urea wash buffer +0.1% Triton X-100; Last time with PBS. Each time of washing was for 5 min. After washing, the nickel beads were eluted with elution buffer (0.2 M imidazole, 0.15 M Tris-HCl [pH 6.8],

30% glycerol, 0.72 M 2-mercaptoethonal, 5% SDS). The elution products were electrophoretically separated by SDS-PAGE, transferred onto a PVDF membrane, probed with an anti-ubiquitin antibody (Abcam), and visualized by ECL Western blotting detection reagent.

Results

A mutant ICP0 lacking residue 343 to 391 leads to partial degradation of PML

In Chapter 2, three ND10-FSs located at ICP0 residues 242 to 291, 343 to 391, and 393 to 441 were identified to facilitate the ND10 fusion of ICP0 redundantly. To assess whether ICP0-ND10 fusion correlates with PML degradation by ICP0, I examined PML levels in cells infected with recombinant viruses containing deletions in the central region of ICP0. I observed residual PML at 8 hpi (lane 5 in Fig 3.2A, panel a) in HEL cells infected with virus RHG113 in which ICP0 lacks residues 343 to 391. The other ICP0 truncations (RHG111, -112, -114, or -115) degraded PML to the same extent as the wild-type ICP0 (RHG101). Interestingly, the PML level in RHG113-infected cells was considerably lower than that in mock- or RHG110-infected cells (lanes 1 and 8 in Fig 3.2A, panel a), suggesting partial PML degradation in cells infected with RHG113. This partial degradation was not because of less ICP0 level in RHG113 infected cells since mutant ICP0 of RHG113 was expressed at similar levels compared with other mutants (lanes 3 to 7 in Fig 3.2A, panel b). PML degradation caused by ICP0 is proteasome-dependent (Chelbi-Alix and de The, 1999). To check whether partial PML degradation is also dependent on proteasome, I added proteasome inhibitor MG132 into RHG113 infected cells. PML level in RHG113 infected cells was similar to that in RHG101 infected cells after MG132 treatment (lanes 4 and 6 in Fig 3.2B, panel a), suggesting that the partial

PML degradation by RHG113 is regulated through the proteasome pathway, too.
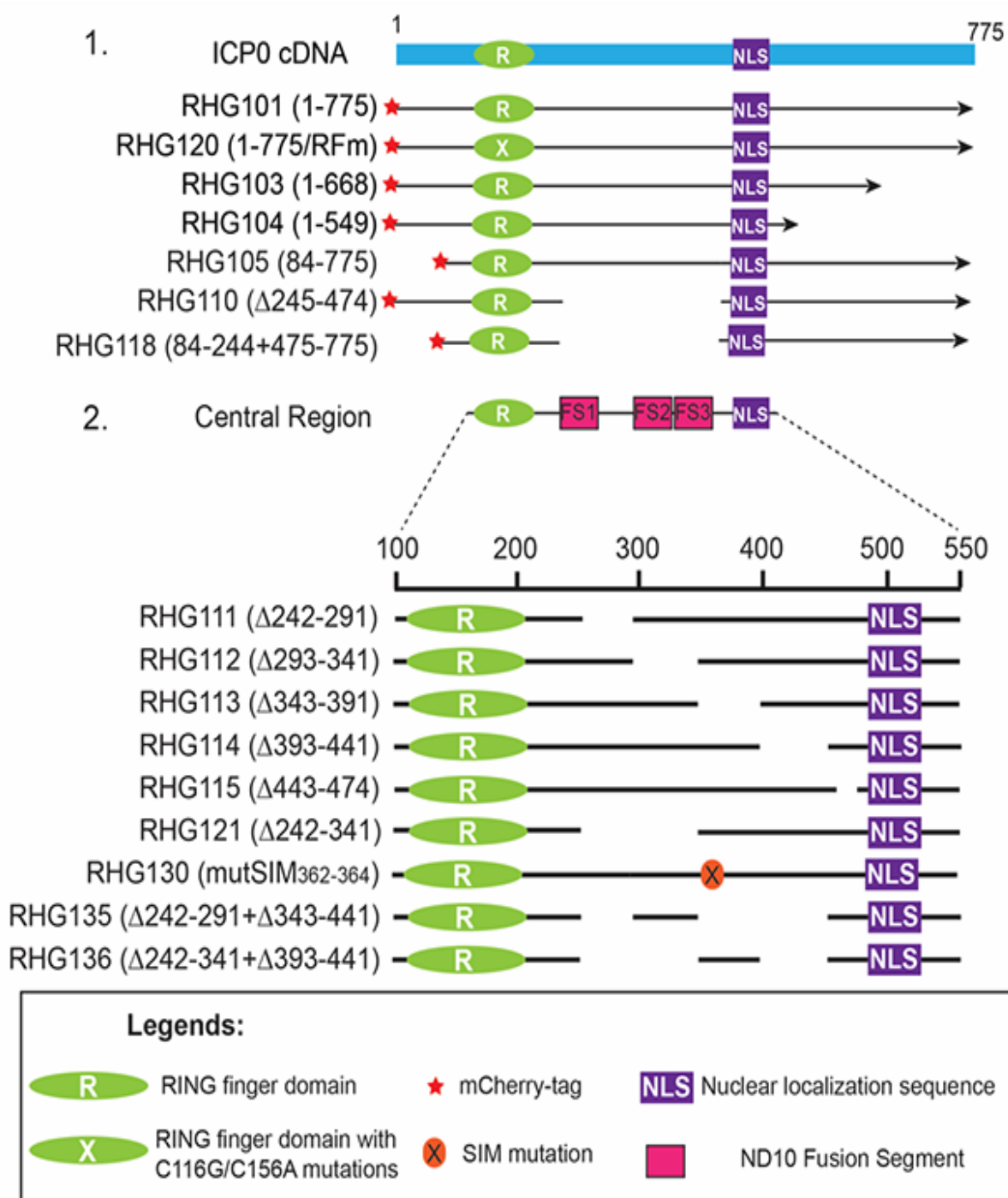
Fig 3.1: Schematic diagrams of ICP0 mutants used in Chapter 3. Line 1, ICP0 cDNA; Line 2, closeup illustration of the central region of ICP0. Amino acid numbers marking the boundaries of these domains are illustrated above the gene. The ICP0s in all of the viruses used in this study are tagged with mCherry. Symbols representing specific domains are shown in the key.
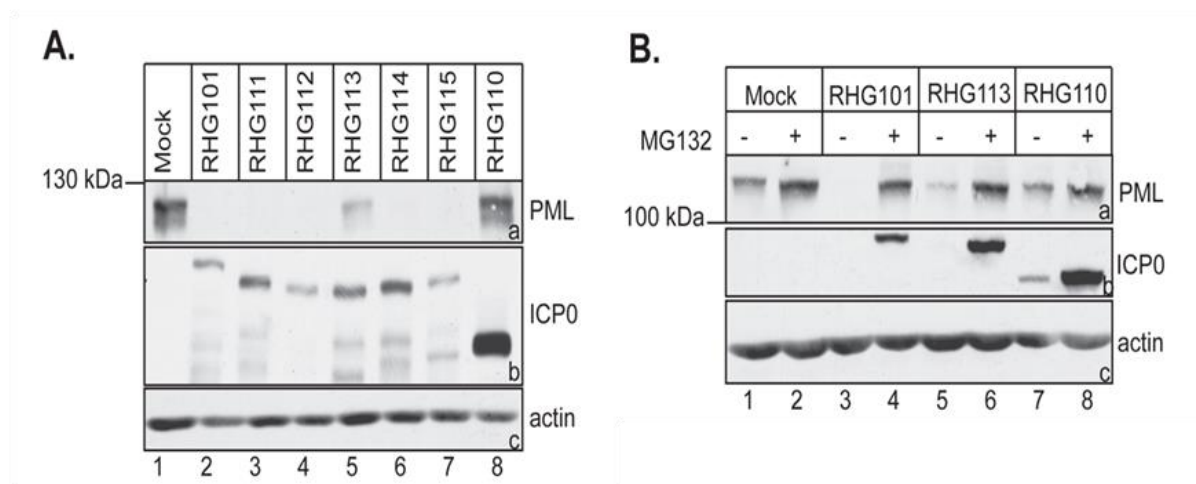
Fig 3.2: ICP0 lacking residues 343-391 causes partial PML degradation. (A) Effect of ICP0 internal deletions on PML degradation. HEL cells were infected with mutant viruses at 10 pfu/cell for 8 h. The total cell lysates were probed in Western blot assays with the antibodies indicated in each gel. (B) Partial PML degradation is proteasome-dependent. HEL cells were pretreated with 10 µM MG132 and then infected with the viruses indicated at 10 pfu/cell in the presence of MG132 for 8 h. Infected cells were lysed, and total cell lysates were probed in Western blot assays with the antibodies indicated in each gel.

ICP0 residues 343 to 391 regulate the degradation of a subset of PML

To check whether partial PML degradation is a delayed degradation that can be completed by increasing enzyme production or reaction time, I adopted two strategies: increasing original MOI and prolonging infection time. Increasing the MOI from 2 pfu/cell to 20 pfu/cell did not substantially enhance PML degradation (lanes 4 and 5 in Fig 3.3A, panel a) in HEL cells. This suggests that degradation of a subpopulation of PML requires residues 343-391 while degradation of another subset PML is independent of residues 343-391. Similar to increasing original MOI, prolonging infection time did not enhance PML degradation in HEL cells (Zheng et al., 2016). I further investigated whether the partial degradation by RHG113 was cell type dependent and found that PML was also partially degraded in RHG113-infected HEp-2 cells. Prolonging the infection time did not

facilitate the degradation in HEp-2 cells (lanes 5 to 7 in Fig 3.3B, panel a), indicating the presence of a similar mechanism that regulates the differential PML degradation in both HEL and HEp-2 cells.
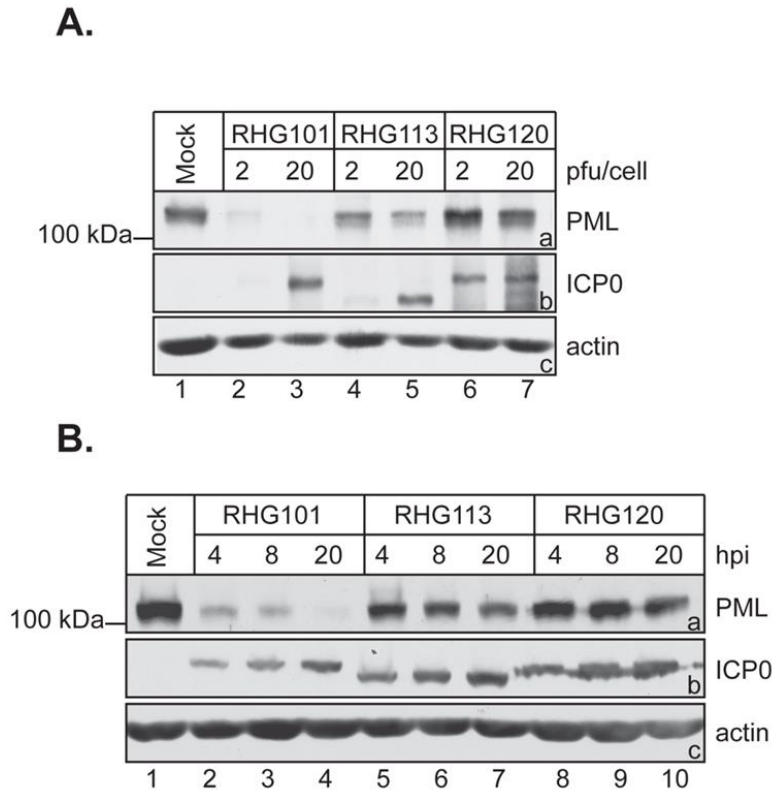
Fig 3.3: ICP0 lacking residues 343-391 causes the degradation of a subset of PML. (A) MOI increase does not enhance partial PML degradation. HEL cells were either mock infected or infected with the indicated viruses at 2 or 20 pfu/cell. Samples were collected at 8 hpi and then subjected to Western blotting as described above. (B) Partial PML degradation was also observed in HEp-2 cells. HEp-2 cells were either mock infected or infected with the indicated viruses with 10 pfu/cell. Samples were collected at indicated time points and then subjected to Western blotting.

**Characterization of HEp-2-TetOn-MycPML I or MycPML II cell lines**

Since a subset of PML degradation is under the regulation of residues 343 to 391 of ICP0, I investigated the seven different isoforms of PML. All of them share the same N-terminus from exon 1 to exon 6 but assemble exons 7 to 9 differently to form the distinct C-termini (Jensen et al., 2001). The polyclonal anti-PML antibody used above recognizes

all the PML isoforms. PML I and PML II have a molecular mass of 100 kDa, matching the size of the partial PML degradation observed in Fig 3.2 and Fig 3.3. Therefore, the hypothesis is that the partial PML degradation is because of a differential degradation of PML I and PML II caused by RHG113. To test our hypothesis, HEp-2-TetOn cells expressing Myc-tagged PML I or PML II were constructed. HEp-2 cell was picked for the construction of stable cell lines based on two reasons. First, HEp-2 cell is much easier to be transfected than HEL cell. Second, partial PML degradation is observed in both HEp-2 and HEL cells. We chose to establish stable HEp-2-TetOn cells expressing MycPML I or MycPML II. There were two reasons for this decision. First, stable cell lines ensure a uniform expression which is suitable for quantitative assays. Second, the TetOn system avoids potential cell alteration induced by long-term PML overexpression during stable cell line selections since PML is a cell cycle regulator (Bernardi and Pandolfi, 2003). After selection, I tested exogenous PML expression. The expression of MycPML I or MycPML II in HEp-2-TetOn cells was tightly controlled, with no detection of MycPML in the absence of Dox (lanes 1 and 5 in Fig 3.4). After 24 h of Dox induction, MycPML was highly expressed and became the major PML population in induced cells (lanes 4 and 8 in Fig 3.4A). Ectopic PML I or PML II colocalized with ND10 bodies represented by another major ND10 component, Sp100, without dramatically changing the morphology of ND10 (Fig 3.4B). These results suggest that we successfully constructed HEp-2 cells expressing MycPML I or MycPML II.

Residues 343-391 of ICP0 are necessary for PML II degradation, not PML I

A half-life assay was established to examine the degradation of MycPML I or MycPML II by ICP0 in early infection (Fig 3.5). Briefly, HEp-2-TetOn cells expressing MycPML I or
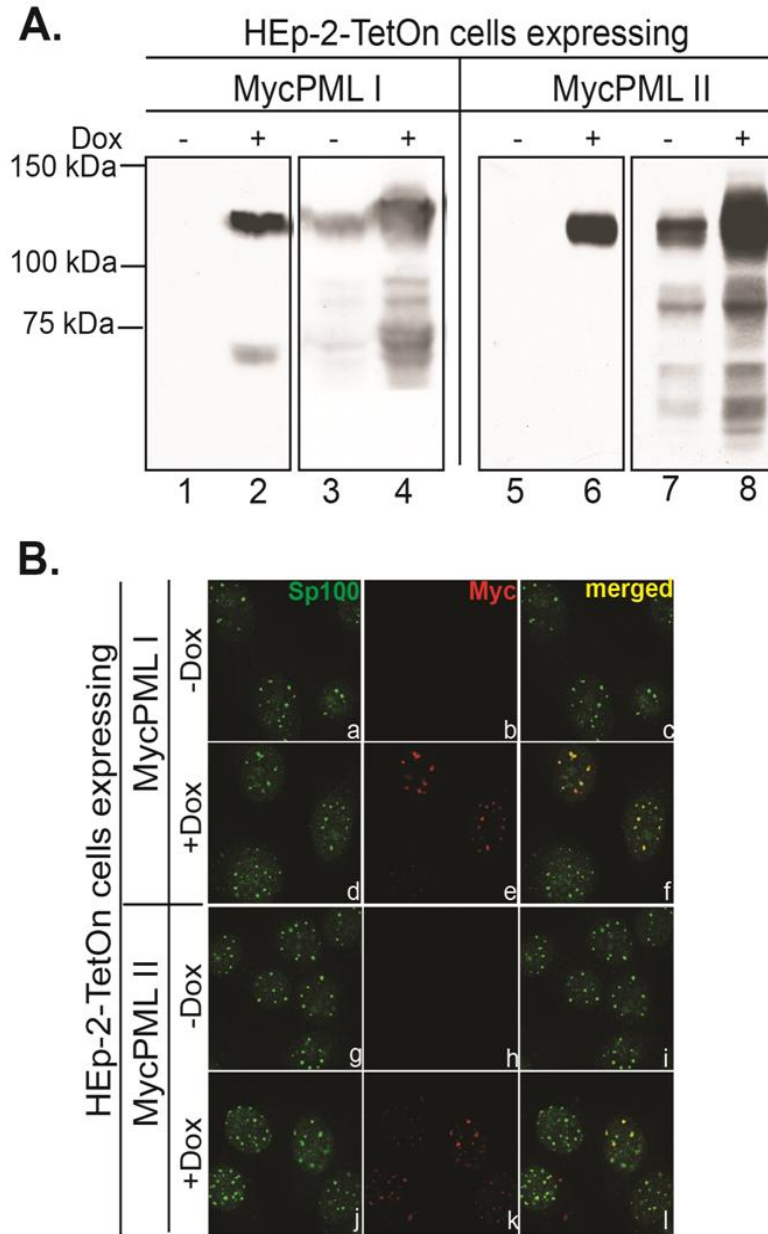
Fig 3.4: Expression and localization of ectopic PML I and PML II in HEp-2-TetOn cells. (A) Comparison of the endogenous PML level and the ectopic MycPML I or MycPML II level in stable cell lines. HEp-2-TetOn cells expressing MycPML I or MycPML II were either mock-induced or induced with 1 µg/ml Dox overnight before the cells were harvested. Total cell lysates were subjected to Western blotting to examine ectopic expression with an anti-Myc antibody and to compare the endogenous and exogenous PML levels with an anti-PML antibody. The values to the left are molecular sizes in kilodaltons. (B) Localization of MycPML I and MycPML II in HEp-2 cells. HEp-2-TetOn cells expressing MycPML I or MycPML II were seeded onto four-well slides and mock-induced or induced as described above. The primary antibodies used to stain cells are indicated at the top of the columns.

MycPML II were induced with Dox to express MycPML I or MycPML II 24 h before

infection. After viral attachment for 1 h, infection inoculum was removed, and infected

cells were incubated in growth medium for another 1 h to allow the initial synthesis of

ICP0. CHX, which is an inhibitor of de novo protein synthesis, was then added. Cells were

harvested afterward at 2-h intervals until 6 h CHX post-treatment. MycPML levels were

quantitated by measuring the band densities from Western blot. The MycPML half-life in

each infection was then calculated by normalizing the PML levels at different time points

against that at the 0-h point, which was set as 100%.
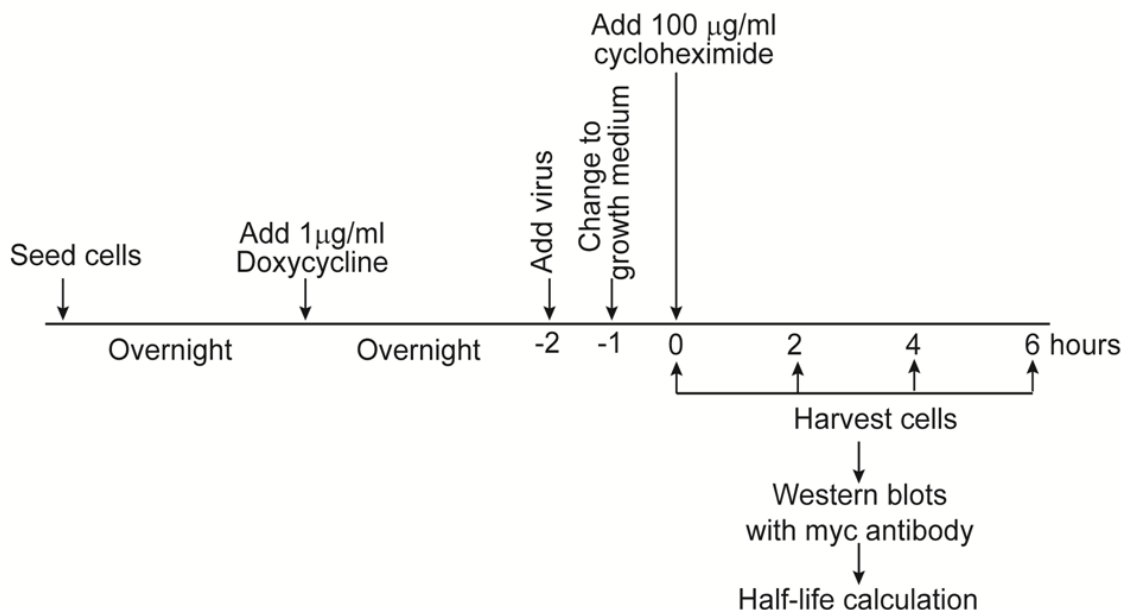
Fig 3.5: Schematic representation of the experimental procedures used to determine PML half-lives. TetOn cells carrying MycPML isoforms were seeded, induced with 1 µg/ml Dox, and then exposed to a test virus at 10 pfu/cell for 1 h. The inoculum was removed, and cells were incubated in growth medium for 1 h before CHX was added. Cells were harvested at 2-h intervals to calculate PML half-lives.

Based on this assay, I individually measured the half-lives of MycPML I and MycPML

II in RHG113-infected cells. RHG113 efficiently degraded MycPML I, comparable to

RHG101 (Fig 3.6, panels b and c). The MycPML I half-life in RHG101- or RHG113-infected cells was shorter than 2 h, whereas it was longer than 6 h in mock-infected cells (Fig 3.6, panel d). However, RHG113 cannot degrade MycPML II (Fig 3.6, panel g). The MycPML II half-life in RHG113 infected cells was longer than 6 h, similar to that in mock-infected cells (Fig 3.6, panel h), whereas wild-type ICP0 again quickly degraded MycPML II (Fig 3.6, panel f), with a half-life shorter than 2 h (Fig 3.6, panel h). These results suggest that partial PML degradation by RHG113 is due to the differential degradation of PML isoforms. Residues 343-391 of ICP0 is necessary for PML II degradation, but dispensable for PML I degradation.
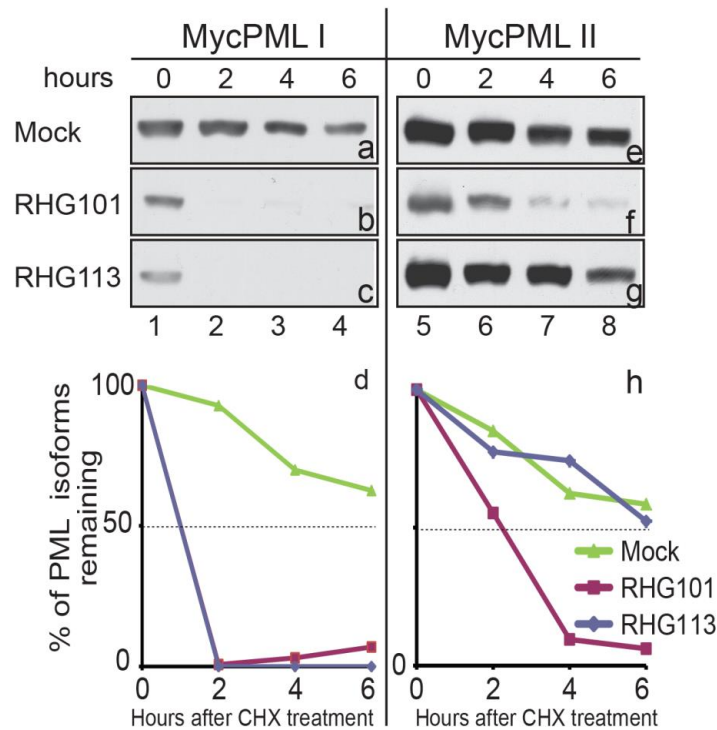
Fig 3.6: ICP0 residues 342-391 are necessary for degradation of PML II, not PML I. Samples taken at the 0-, 2-, 4-, and 6-h points were probed with an anti-Myc antibody in Western blot assays. HEp-2 cells expressing PML isoforms and the time points are indicated above the gel strips. Virus names (or mock infection) are listed to the left of the gels. Band densities were quantified by ImageJ, and PML half-lives are plotted below the corresponding gels.

PML protein level change is not caused by PML mRNA level change during infection

In Fig 3.6, the MycPML II level at the 0-h point in RHG113 infected cells was similar to that in mock-infected cells (lane 5 in Fig 3.6, panels e and g). However, the MycPML II level at the time of cycloheximide addition (0 h timepoint in Fig 3.5) in RHG101 infected cells was significantly lower than that in mock-infected cells (lane 5 in Fig 3.6, panel f). Similarly, MycPML I level at the 0-h point in RHG101 and RHG113 infected cells were significantly lower than that in mock-infected cells (lane 1 in Fig 3.6, panels a to c). This phenomenon is likely because upon its synthesis, ICP0 quickly leads to PML degradation prior to addition of cycloheximide.
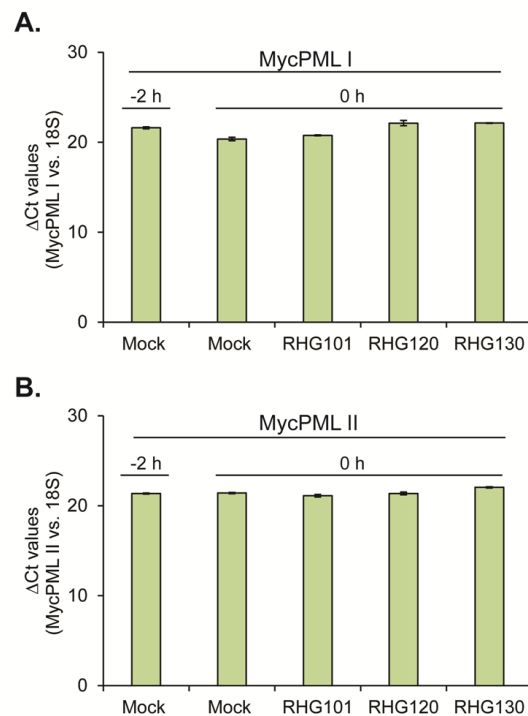
Fig 3.7: No substantial changes were observed in MycPML I or MycPML II mRNA level at −2- or 0-h in infections. HEp-2-TetOn cells expressing MycPML I (A) or MycPML II (B) were induced and infected with the viruses indicated. At −2 and 0 h, total RNA was extracted, cDNA was synthesized, and quantitative RT-PCR was performed to detect MycPML isoforms. The cycle threshold (ΔCt) number of MycPML was normalized against the18S rRNA.

To rule out the possibility that PML protein level change is because of transcriptional regulation, I examined the mRNA levels of MycPML I and MycPML II. I found minimal changes of mRNA at 0-h time point in cells infected with different viruses compared with -2-h time point in mock-infected cells (Fig 3.7A and B), indicating that the difference observed in protein levels of MycPML between -2-h and 0-h point is through posttranslational modification.

SIM$_{362-364}$ located within residues 343-391 of ICP0 is critical for PML II degradation, but not PML I

As described in Chapter 2, SLS4 is responsible for the interaction with SUMO-2/3 and the ubiquitination of a poly-SUMO-2 substrate in vitro (Boutell et al., 2011). The recombinant virus containing a mutant SLS4 has been shown to be able to degrade PML isoform I but not SUMOylated isoform II in the absence of all endogenous PMLs (Everett et al., 2014). SLS4 (our lab named it SIM$_{362-364}$) resides within residues 343-391 of ICP0. To test whether SIM$_{362-364}$ is responsible for the differential PML degradation observed above, I built the recombinant virus RHG130, in which ICP0 contains the mutations of I362G, V363A, and I364G, and examined its degradation of MycPML I and MycPML II. To further exclude potential variations caused by virion tegument proteins or other immediate early viral proteins, recombinant virus RHG120, which contains C116G/C156A substitutions and completely loses the E3 ligase activity (Gu et al., 2013), was used as the non-degradation control (Fig 3.8A, panels a and e). RHG130 with ICP0 containing mutated SIM$_{362-364}$ degraded MycPML I to the same extent as the wild-type ICP0 (Fig 3.8A, panels b and c) and showed a half-life shorter than 2 h (Fig 3.8A, panel d). Moreover, RHG130 was not capable of degrading MycPML II (Fig 3.8A, panel g),
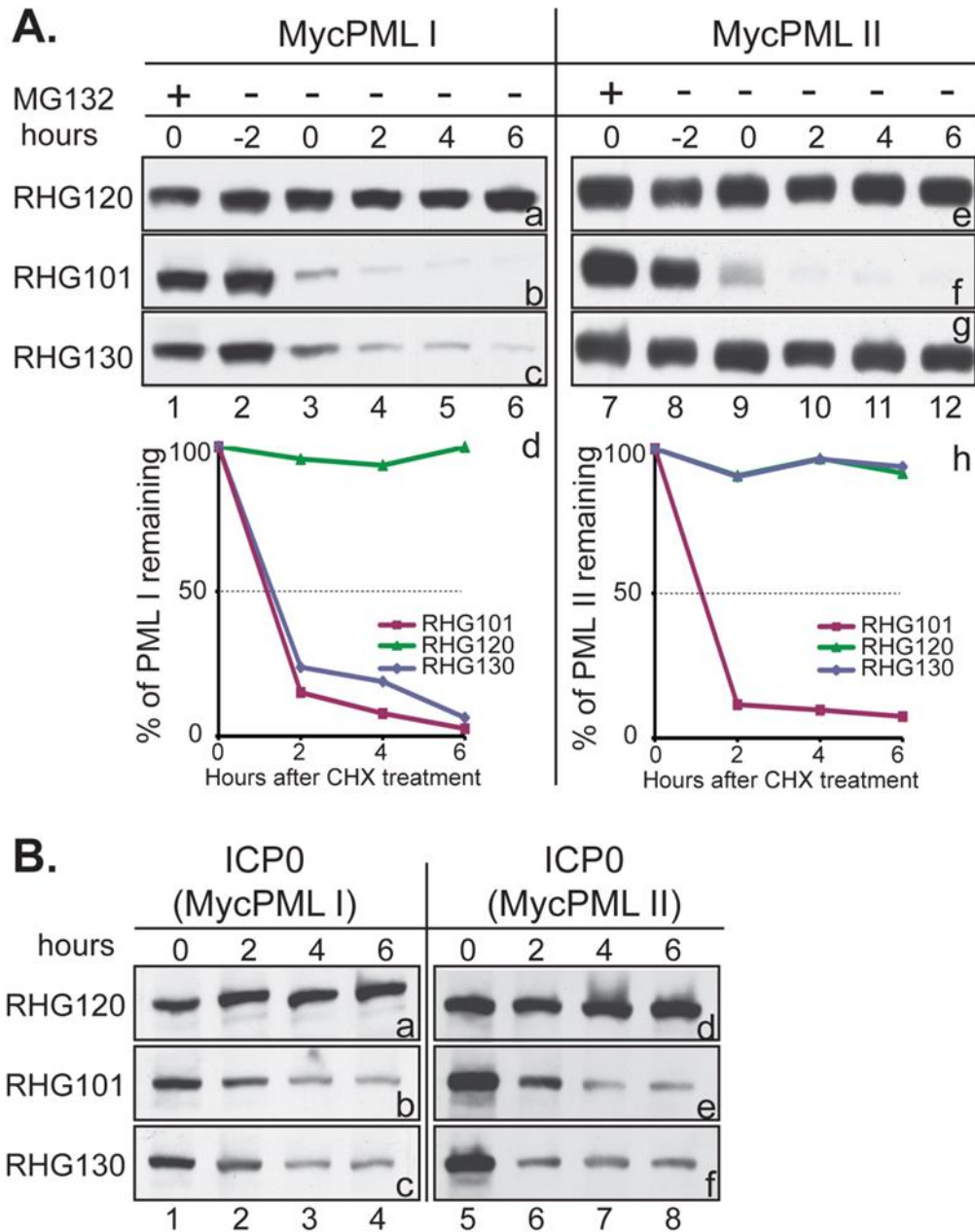
Fig 3.8: SIM$_{362-364}$ is essential for the degradation of PML II, but not for that of PML I. (A) HEp-2-TetOn cells expressing MycPML I or MycPML II were infected with the viruses indicated in the presence or absence of MG132. Samples were taken for Western blotting with an anti-Myc antibody, and the half-lives of PML isoforms were calculated as described above. (B) The same samples shown in panel A were probed with an anti-mCherry antibody in Western blot assays.

consistent with what was observed in RHG113 infected MycPML II cells. The half-life of

MycPML II in RHG130-infected cells was longer than 6 h, similar to that of the E3 inactive

mutant (RHG120) (Fig 3.8A, panel h). In this experiment, a −2-h sample for each testing virus was also examined to show that PML isoforms were induced to a comparable level before the test virus was added (lanes 2 and 8 in Fig 3.8A). Also, MG132 was added to one of the parallel infections at −2 h along with the virus, and those cells were harvested at 0 h. The proteasomal inhibition between −2 and 0 h prevented the degradation of MycPML (lanes 1 and 7 in Fig 3.8A). Therefore, the decrease in the MycPML I or MycPML II level at the 0-h point in infections where ICP0 was capable of degrading the PML isoform was indeed the result of PML degradation by the newly synthesized ICP0. Based on these observations, two criteria were used to evaluate the ability of a mutant ICP0 to degrade PML isoforms: First, whether degradation occurs between the −2- and 0-h points before the CHX treatment. Second, whether the PML isoform half-life in ICP0 mutant virus infected cells is comparable to the full degradation control.

To rule out the possibility that differences in PML degradation are the result of different amounts of ICP0 expressed, I also examined ICP0 levels in the respective infections. The result showed that ICP0 levels were comparable at 0 h (lanes 1 and 5 in Fig 3.8B) and ICP0 half-lives were similar in RHG101 and RHG130 infected cells (Fig 3.8B, panels b, c, e, and f). The similar initial levels and turnover rates of ICP0 indicate that the differentiation in PML I and II degradation is because of the I362G, V363A, and I364G substitutions.

$SIM_{362-364}$ is not sufficient for PML II degradation

Since $SIM_{362-364}$ is essential for MycPML II degradation, the next question is whether it is sufficient for degradation of MycPML II. To test this, I used RHG136 that only contains residues 343 to 391 in ICP0 central region. RHG136 failed to resuscitate MycPML II

degradation (Fig 3.9A, panel d) through half-life assay, suggesting SIM$_{362-364}$ is not sufficient for PML II degradation.
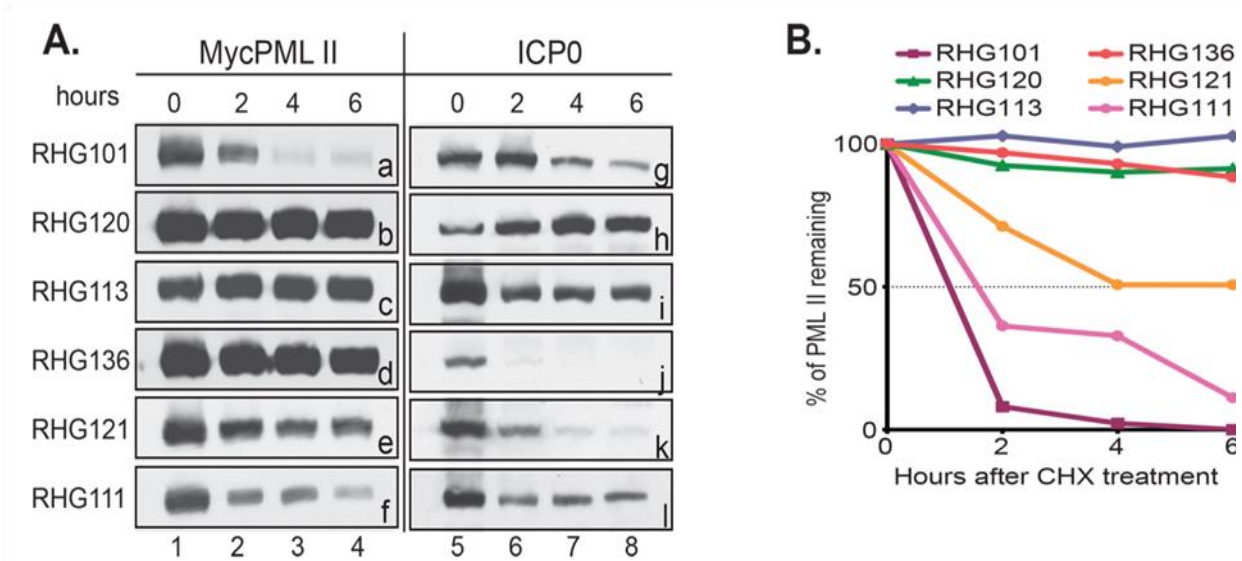
Fig 3.9: Residues 343-391 of ICP0 coordinate with the proximal sequences to regulate PML II degradation. (A) HEp-2-TetOn cells expressing MycPML II were induced, infected with the viruses indicated, and harvested for Western blotting. The left panel was probed with anti-Myc antibody to check PML II level, while the right panel was probed with anti-mCherry antibody to check ICP0 level. (B) The band densities in the MycPML II blot (left panel in A) were quantified through ImageJ. The PML II half-lives were determined as described in Fig 3.6.

The half-life of MycPML II was more than 6 h in RHG136 infected cells, similar to that in RHG120 and RHG113 infected cells (Figure 3.9B). Interestingly, when the surrounding sequences of residues 343 to 391 were restored (RHG121 and RHG111), MycPML II degradation was partially restored (Fig 3.9A, panels e and f). The half-life of MycPML II was close to 4 h in RHG121 infected cells and it was shortened to about 2 h in RHG111 infected cells (Figure 3.9B), indicating that sequences in the proximity of residues 343 to 391 are also important for active PML II degradation to occur.

C-terminus of ICP0 is also essential for efficient PML II degradation

Previously, C-terminus of ICP0 has been implicated in affecting PML degradation

(Gu and Roizman, 2009). To assess whether MycPML II degradation is also affected by C-terminal sequences, I used recombinant viruses RHG103 and RHG104, which contain ICP0 lacking the C-terminal 107 and 226 amino acids, respectively. RHG103 and RHG104 failed to degrade MycPML II (Fig 3.10, panels c and d) through half-life assay, consistent with a previous report showing that ICP0 with the C-terminal 181 amino acids deleted did not degrade SUMOylated PML II (Cuchet-Lourenco et al., 2012). This observation suggests C-terminal sequences of ICP0 are also necessary for efficient PML II degradation to happen, in addition to SIM$_{362-364}$ and sequences proximal to residues 343 to 391.
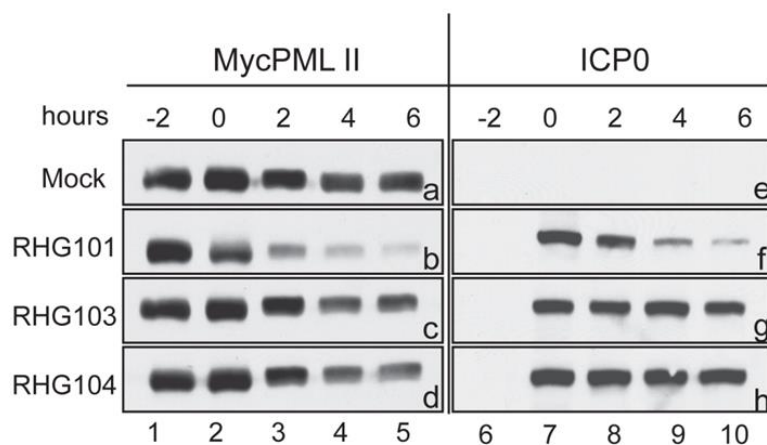
Fig 3.10: C-terminal sequences also regulate PML II degradation. HEp-2-TetOn cells expressing MycPML II were induced, infected by the viruses with the C-terminal truncation of ICP0, and harvested at indicated time points for Western blotting.

Failure of PML II degradation affects viral genome replication

To further understand the biological significance of the inability to degrade a particular set of PML isoforms, I examined the impact of deletion of residues 343 to 391 on viral genome replication. The qPCR analysis result showed that viral DNA had a 2,624-fold increase for RHG101 at 24 hpi but only a 780-fold increase for RHG113, just slightly

higher than the 610-fold increase for RHG120 (Fig 3.11A) in HEp-2-TetOn cells expressing MycPML II. To exclude the replication differences caused by the variations in viral inputs, viral DNA amounts at 2 hpi were measured and compared. Significant differences were not found (Fig 3.11B), suggesting that the inability of RHG113 to degrade PML II greatly impairs its viral DNA replication.
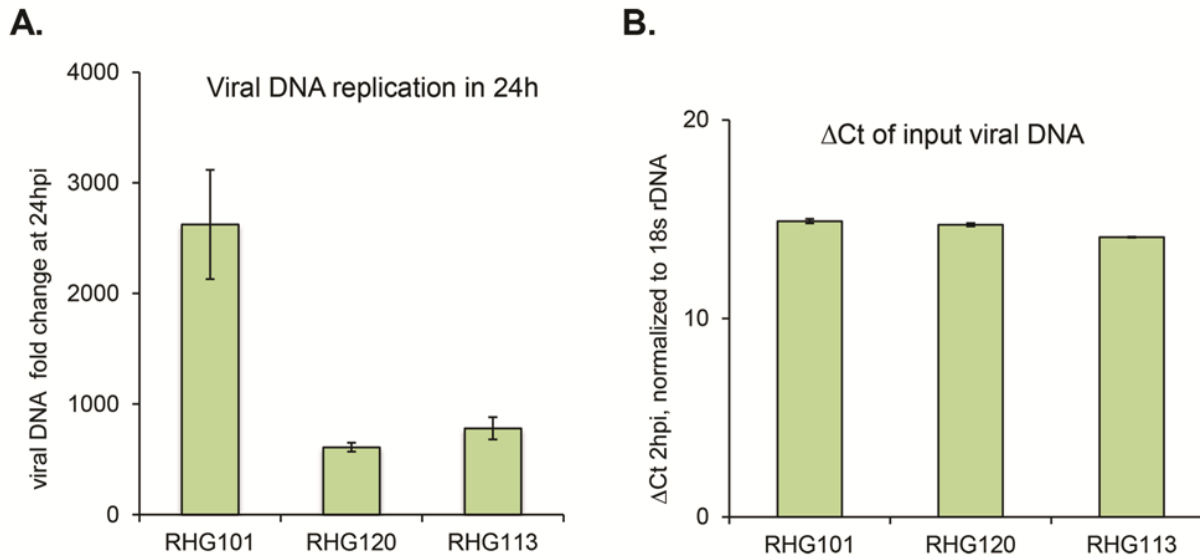
Fig 3.11: Failure of PML II degradation affects viral genome replication. (A and B) HEp-2-TetOn cells expressing MycPML II were induced and infected with the viruses indicated at 0.1 pfu/cell. Total DNAs extracted at 2 and 24 hpi were subjected to qPCR with primers targeting the ICP27 or 18S rRNA gene to calculate the viral DNA fold increase within 24 h. Viral DNA fold increases of the 24-h samples relative to the 2-h samples were plotted by the ΔΔCT method (A). The cycle numbers for 2-h viral DNA normalized against 18S rDNA (ΔCT) were plotted (B).

PML I degradation is not affected by ICP0-ND10 fusion

Since SIM is not essential for PML I degradation, the next question is what is the sequence requirement in ICP0 for PML I degradation. Two potential mechanisms may regulate the degradation of PML I. First, ND10 fusion controls the spatial localization of ICP0 and presumably regulates its access to PML I and affects its substrate degradation.

Second, specific sequences in ICP0 are required to target PML I for proteasomal degradation.

To test whether ND10 fusion process affects PML I degradation or not, I used ND10 fusion-competent virus RHG136 and fusion-incompetent virus RHG135. ICP0 in RHG135 bearing the deletion of all three ND10 fusion segments (ND10-FSs) cannot fuse with ND10 while ICP0 in RHG136 having ND10-FS2 can fuse with ND10 (Zheng and Gu, 2015). Both RHG135 and RHG136 actively degraded MycPML I, compared to the non-degradation control RHG120 and the full degradation control RHG101 (Figure 3.12). This phenomenon suggests that ND10 fusion is not responsible for degradation of PML I, and ICP0 probably degrades PML I both inside and outside ND10 bodies.
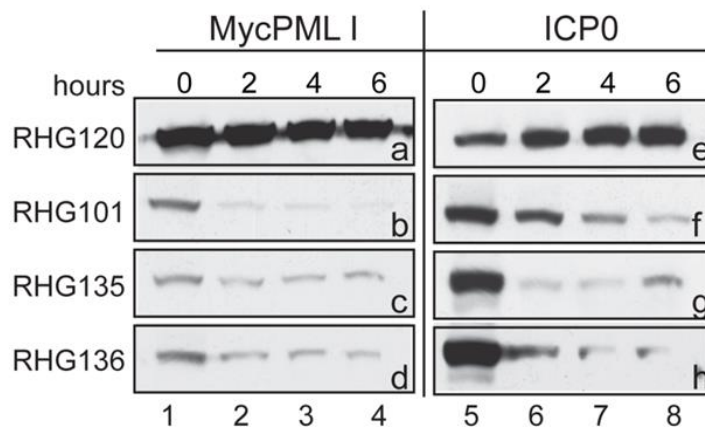
Fig 3.12: The ND10 fusion ability of ICP0 does not affect PML I degradation. HEp-2-TetOn cells expressing MycPML I were induced, infected with the indicated viruses, and harvested at indicated time points for Western blotting.

C-terminus of ICP0 plays a minimal role for PML I degradation

To identify elements responsible for regulating PML I recognition and degradation, I performed deletion mapping and started from the viruses with the C-terminal truncation of ICP0. In contrast to MycPML II, MycPML I can be degraded by RHG103 and RHG104

with slight delays compared with wild-type ICP0 (Fig 3.13A, panels c and d). The MycPML

I half-lives in RHG103- and RHG104-infected cells were 2 to 4 h (Fig 3.13B), indicating

that PML I degradation is independent of the C-terminus of ICP0.
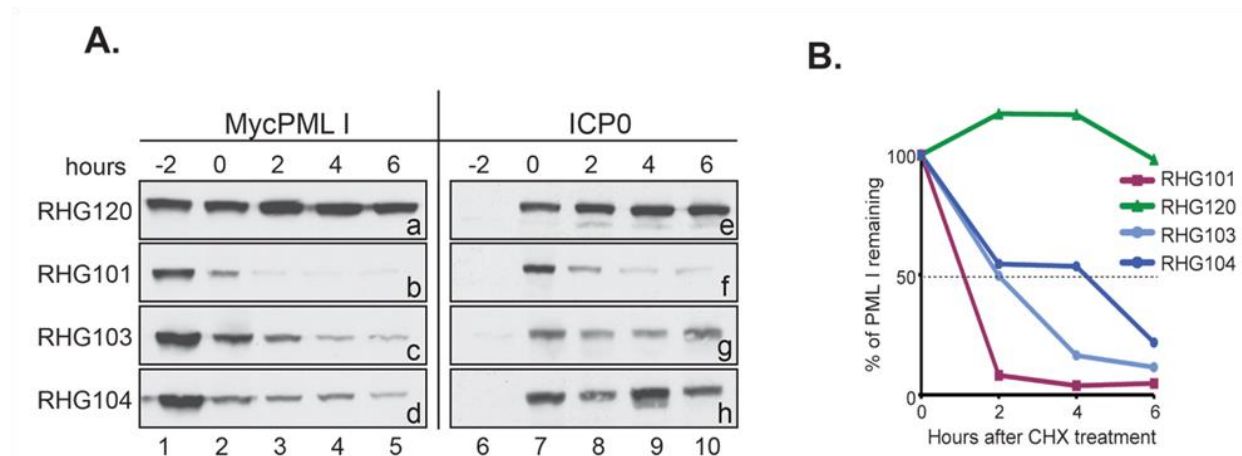
Fig 3.13: C-terminus of ICP0 is not essential for PML I degradation. (A) HEp-2-
TetOn cells expressing MycPML I were induced, infected with the C-terminal
truncation viruses, and harvested for Western blotting with the indicated antibodies.
(B) The band densities in the MycPML I blot (left panel in A) were quantified through
ImageJ. The MycPML I half-lives were determined as described in Fig 3.6.

Bipartite domains in the N-terminus of ICP0 coordinate to regulate the degradation

of PML I

Since the C-terminus of ICP0 is not critical for degradation of PML I, I conducted

additional deletion mapping to examine whether the N-terminal domains are necessary

for MycPML I degradation. N-terminal residues 1 to 83 and internal residues 245 to 474

are the sequences flanking the RING domain but not participating in the formation of the

C3HC4 RING (Everett et al., 1993). Therefore, I used recombinant viruses RHG105

(single deletion of residues 1 to 83), RHG110 (single deletion of residues 245 to 474),

and RHG118 (double deletion of both residues 1 to 83 and 245 to 474) to map the N-

terminal region of ICP0. In the MycPML I half-life assay, MycPML I levels at 0 h in both

RHG105- and RHG110-infected cells were significantly lower than that at −2 h, suggesting MycPML I degradation occurred between the −2- and 0-h points (lanes 1 and 2 in Fig 3.14A, panels c and d). However, I did not observe progressive loss of MycPML I in either RHG105- or RHG110-infected cells after CHX was added to each infection (lanes 2 to 5 in Fig 3.14A, panels c and d). Examination of the mutant ICP0 level revealed that ICP0 disappeared quickly after CHX treatment in both RHG105- and RHG110-infected cells (lanes 7 to 10 in Fig 3.14A, panels h and i). The drastic loss of ICP0 in the absence of residues 1 to 83 or residues 245 to 474 resulted in the elimination of ICP0 E3 ligase activity upon CHX treatment and presumably prevented the continuous degradation of MycPML I. In RHG118-infected cells, double deletions of residues 1 to 83 and residues 245 to 474 completely abolished MycPML I degradation. I observed neither a decrease in MycPML I between the −2- and 0-h points nor progressive disappearance of MycPML I (Fig 3.14A, panel e), as in RHG120-infected cells (Fig 3.14A, panel a). This phenomenon suggests that two regions (residues 1 to 83 and residues 245 to 474) in ICP0 cooperate to regulate PMLI degradation. Only when both bipartite regulatory domains are deleted is PML I degradation blocked.

To further confirm that the loss of progressive degradation after CHX treatment resulted from the fast turnover rate of the mutant ICP0, I performed another experiment in the absence of CHX to accumulate mutant ICP0. The result showed that MycPML I was progressively degraded in RHG105 and RHG110 infected cells (lanes 2 to 4 in Fig 3.14B, panels c and d). RHG101 could cause continuous degradation of MycPML I as expected, with a faster degradation rate compared with RHG105 and RHG110 (lanes 2 to 4 in Fig 3.14B, panel b). RHG118 cannot degrade MycPML I even with the accumulation of ICP0

(lanes 2 to 4 in Fig 3.14B, panel a). This phenomenon confirms the hypothesis that the bipartite motifs necessary for recognition and degradation of PML I reside in residues 1 to 83 and residues 245 to 474. Mutant ICP0 with the presence of either motif alone still lead to PML I degradation.
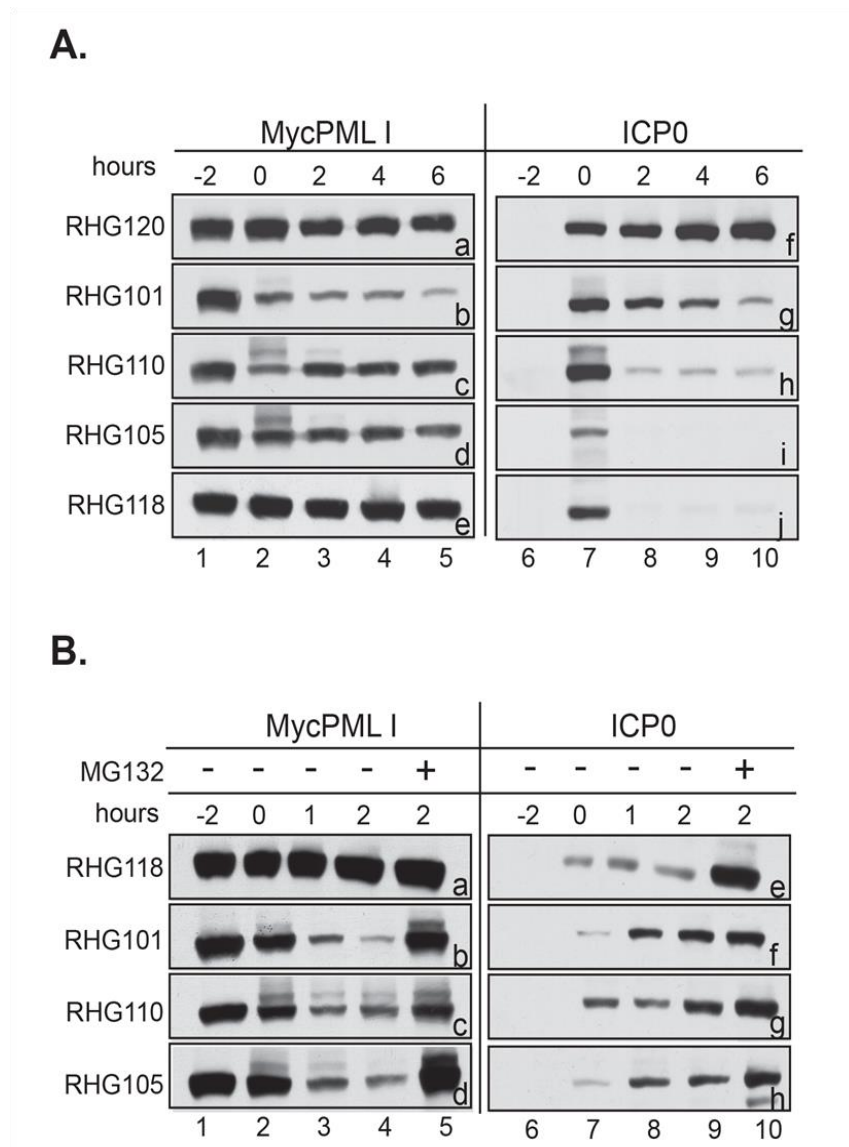
Fig 3.14: Bipartite domains in the N-terminus of ICP0 coordinate PML I degradation. (A) HEp-2-TetOn cells expressing MycPML I were induced, infected with the N-terminal truncation viruses, and collected for Western blotting. Samples harvested after 0 h time point were treated with CHX as previously described. (B) HEp-2-TetOn cells expressing MycPML I were infected with the N-terminal truncation viruses in the absence of CHX and harvested at the indicated time points for Western Blotting.

An interesting phenomenon is the accumulation of modified MycPML I with slower mobility at the 0-h point in both RHG105- and RHG110-infected cells (lane 2 in Fig 3.14A, panels c and d). The modified MycPML I was not observed in the non-degradation control (RHG120) and RHG118-infected cells (lane 2 in Fig 3.14A, panels a and e). MG132 treatment enhanced the modified MycPML I bands in RHG101, RHG105 and RHG1110 infected cells (lane 5 in Fig 3.14B, panels b to d), suggesting that the MycPML I ubiquitination is likely not affected, but degradation is considerably delayed in the presence of only one of the bipartite MycPML I interacting domains.

Mutant ICP0 lacking residues 1 to 83 or residues 245 to 474 is capable of polyubiquitinating PML I

The MycPML I levels at 0 h in both RHG105- and RHG110-infected cells were significantly lower than that in the −2-h sample, suggesting MycPML I degradation occurred between the −2- and 0-h points. In addition, the presence of slower mobility bands of MycPML I in RHG105 and RHG110 infected cells suggests that RHG105 and RHG110 can ubiquitinate MycPML I. To confirm this, I performed a pull-down assay using nickel beads since there is a His-tag in front of MycPML I. The enriched MycPML I was probed with an anti-ubiquitin antibody to test whether RHG105 and RHG110 can indeed polyubiquitinate MycPML I. As shown in Fig 3.15, nickel beads can efficiently pull down HisMycPML I (Fig 3.15A, compare lane 3 with lane 1). A strong signal of polyubiquitinated HisMycPML I (lane 7 in Fig 3.15A) following the pull-down assay suggests that ICP0 in RHG105 can polyubiquitinate HisMycPML I. I also tested the specificity of the pull-down by comparing the ubiquitin signal in the presence of HisMycPML I with that in the absence of HisMycPML I. A much weaker ubiquitin signal in the pull-down sample in the absence

of HisMycPML I expression (Fig 3.15A, compare lane 7 with lane 8) indicates the high specificity of the pull-down assay.
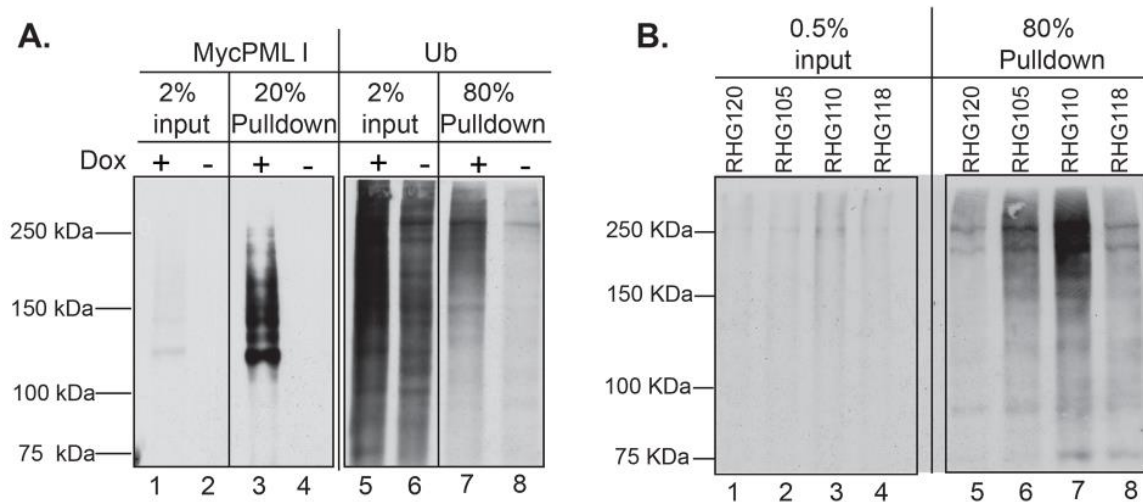
Fig 3.15: ICP0 mutant with either arm deleted can polyubiquitinate PML I. (A) HEp-2 TetOn cells expressing MycPML I were either mock-induced or induced with Dox as described above. Cells were then infected with RHG105 at 10 pfu/cell. At 2 hpi, cells were harvested for His-tag purification. Lysates and elutes were probed with anti-Myc antibody and anti-ubiquitin antibody. (B) HEp-2 TetOn cells expressing MycPML I were induced as described above. Cells were then infected with indicated viruses at 10 pfu/cell. At 2 hpi, cells were harvested for His-tag purification. Lysates and elutes were probed with anti-ubiquitin antibody.

By performing a pull-down assay, I also evaluated the polyubiquitination level of HisMycPML I by RHG110. To rule out the polyubiquitination of HisMycPML I caused by other infection events instead of ICP0 E3 activity, I used RHG120 as the negative control. RHG120 cannot polyubiquitinate HisMycPML I (lane 4 in Fig 3.15B), consistent with the fact that RHG120 completely lose its E3 ubiquitin ligase activity. Results in Fig 3.15B showed that both RHG105 and RHG110 were capable of polyubiquitinating HisMycPML I (lanes 5 and 6 in Fig 3.15B), consistent with their capability to degrade HisMycPML I.

Discussion

ICP0 is employed by HSV-1 to disarm host antiviral responses through either degrading

restrictive factors or directly interacting with regulatory complexes (Gu, 2016; Gu and Zheng, 2016). ICP0 manipulates and counteracts multiple cellular pathways for efficient viral gene expression. However, the cooperativity of its functional domains is not clearly understood. In this study, I focused on elucidating how different elements of ICP0 regulate its E3 ubiquitin ligase activity. Two distinct mechanisms have been identified for ICP0 to distinguish two of its substrates, PML I and PML II.

First, SIM is necessary, but not sufficient for PML II degradation. ICP0 with a SIM mutation failed to degrade PML II, suggesting that SUMOylation of PML II is likely critical for ICP0 recognition. Degradation of PML II bearing mutations on SUMOylation sites will help us to determine whether SUMOylation of PML II or SUMOylation of other ND10 components is the determinant. My results have indicated that the SIM alone is not sufficient for PML II degradation. Proximal sequences surrounding $SIM_{362-364}$ of ICP0 and distal sequences located at the ICP0 C-terminus were both involved in supporting progressive PML II degradation, suggesting that the overall structure surrounding $SIM_{362-364}$ of ICP0 is likely necessary for ICP0 to ubiquitinate and degrade PML II, even when $SUMO-SIM_{362-364}$ is intact. A previous study found that the specificity and affinity of SIM-SUMO interaction are enhanced by phosphorylation of serine residues right after SIM motif (Stehmeier and Muller, 2009). In the case of $SIM_{362-364}$, residues IVI are followed by SDS. The previous study has suggested that these three residues SDS regulate PML degradation by ICP0 in a transfection assay (Boutell et al., 2008). These observations indicate that $SIM_{362-364}$/SUMO recognition is likely phosphorylation-dependent. To prove this, we can mutate the residues SDS to see whether ICP0 degradation of PML II is affected or not.

Bipartite ICP0 domains located upstream and downstream of the RING finger, instead of SUMO-SIM362–364 interaction, coordinate active PML I degradation. The Co-IP assay also showed that the bipartite domains were responsible for the ICP0-PML I interaction (Zheng et al., 2016). ICP0 with the deletion in either arm could cause the PML I level to decrease between -2-h time point and 0-h time point. However, the decrease did not progress after addition of CHX due to the quick degradation of ICP0 in the presence of CHX. Consistent with this hypothesis, ICP0 with either arm deletion led to continuous PML I degradation without CHX. Mutant ICP0 with deletions in both arms could not bind to PML I and therefore failed to recognize and degrade PML I in the presence or absence of CHX. Through an *in vivo* ubiquitination assay, mutant ICP0 with either arm deleted polyubiquitinated PML I, consistent with the fact it can cause PML I degradation. However, mutant ICP0 causes the accumulation of modified PML I, which is not shown in wild-type ICP0. Several possible reasons may explain this phenomenon. First, mutant ICP0 have a slower rate of polyubiquitination than wild-type ICP0, which leads to the accumulation of modified PML I bands. Second, the polyubiquitin linkage attached to PML I by ICP0 mutant is different from that by wild-type ICP0. The mutant ICP0 polyubiquitinates PML I with a mixture of polyubiquitin chains and a certain fraction of polyubiquitin chains signal for proteasome degradation differently. The exact mechanism needs further investigation.

Naturally, the next interesting question is why ICP0 treats individual substrates differently. One possible reason is the different biochemical features of these substrates. For example, individual PML isoforms may occupy different premises of ND10, such as the ND10 surface or core area. Structural study of ND10 has reported that 50% of

SUMO2/3 is in ND10 core area (Lang et al., 2010). Since SIM$_{362-364}$ is necessary for SUMO2/3 interaction and PML II degradation, PML II probably occupies the core area of ND10. Different from PML II, PML I is degraded regardless of whether ICP0 can fuse with ND10 or not. This phenomenon suggests PML I may have a fast exchange rate between ND10 and nucleoplasm and PML I degradation occurs regardless of PML I location.

Another possible reason for ICP0 to recognize its substrates differently can be that the roles these substrates play in HSV-1 infection are entirely different. Xu et al. showed that PML gene knockout via CRISPR/Cas causes reduced induction of Sp100 upon interferon treatment but also causes wild-type HSV-1 to replicate ineffectively, suggesting that the PML gene products have both positive and negative influences on HSV-1 replication (Xu et al., 2016). That ICP0 uses different mechanisms to degrade PML isoforms may be a result of an evolutionary adaptation of HSV-1 to host responses by causing degradation of restrictive factors and at the same time gathering advantageous factors via protein-protein interaction, which can be regulated by differential polyubiquitination.

PML I and PML II share the same N-termini and differ in their C-termini. Both have antiviral functions and inhibit HSV-1 replication (Cuchet et al., 2011). However, their C-termini specify their unique activities. PML I has a nuclear export sequence (Henderson and Eleftheriou, 2000) and nucleolar targeting sequence, which facilitate its targeting to nucleolar caps in stressed or senescent cells (Condemine et al., 2007). Different from PML I, the C-terminal region of PML II has a secondary and redundant NLS separate from the NLS shared by other isoforms in exon 6 (Jul-Larsen et al., 2010). In addition to the secondary NLS, the C-terminus of PML II also has a nuclear periphery targeting sequence responsible for nuclear envelope localization and essential for liquid droplet

(LD) formation (Ohsaki et al., 2016). The C-terminus of PML I interacts with AML1 (acute myeloid leukemia) and recruits it to PML nuclear bodies together with p300 (Nguyen et al., 2005). All of these findings suggest that their unique C-termini determine their distinct cellular localization under certain stimulation and different interaction partners. Therefore, PML isoforms may play distinct roles in different pathways during viral infection, which requires ICP0 to target them differently. We need to carefully investigate the specific role of PML I and PML II during viral replication in the future.

By establishing a half-life assay to test substrate degradation, we laid a foundation for examining the degradation of other substrates. PML IV and PML VI degradation have been studied and found to be $SIM_{362-364}$-dependent (Zheng et al., 2016). In the future, such substrates can be tested through this assay to further dissect the sequences in ICP0 for counteracting a particular substrate. Through this work, we will be able to delineate ICP0 functional domains in substrate recognition, which has the potential to help us in designing a drug that targets ICP0 to block viral replication.

CHAPTER 4 FUTURE DIRECTIONS

In Chapter 2, I identified three proline-rich segments in ICP0 that independently drive ICP0 to fuse with ND10. This study pinpointed the specific sequences regulating the interaction between ICP0 and ND10. In Chapter 3, I identified elements in ICP0 that control recognition of PML isoforms. This study defined the sequences in ICP0 essential for its substrate differentiation and regulation of its E3 ubiquitin ligase activity. Through both studies, I mapped the sequences in ICP0 mediating the interaction between ICP0 and ND10 and regulating the degradation of ND10 components by ICP0. However, some outstanding questions need to be answered in the future studies regarding both projects.

Does the proline-rich ND10 fusion segment form PPII helix secondary structure and do the proline residues play critical roles in driving ND10 fusion?

The redundant ND10-fusion segments share high proline percentage. The proline-rich sequences have the propensity to form a secondary structure of PPII helix. ICP0 residues 245 to 510, which contain ND10-ES for ND10 fusion step, possess multiple SH3 domain binding sites, which mediate the interaction with SH3 domains of CIN85 (Liang et al., 2005), suggesting ND10-fusion segments likely form PPII helix structure. To prove this, a peptide containing about 10 residues and spanning the proline-rich region within one ND10-fusion fragment can be synthesized and crystallized for protein structural analysis. There have been multiple reports about structural analysis of proline-rich motifs (Bacarizo et al., 2015; Musacchio et al., 1994). The first crystal structure of an oligoproline adopting an all trans PPII helix conformation was presented recently (Wilhelm et al., 2014). In that study, Wilhelm et al. reported variety of aqueous and nonaqueous solvents that were not successful for obtaining crystals suitable for X-ray analysis. Crystallization was finally

achieved in hexaproline, which has a p-bromobenzoyl moiety at its N-terminus and a carboxylic acid group at its C-terminus. Therefore, the challenge in this project is to obtain a crystal of ND10 fusion segment peptide fit for structural study. To overcome this, we can separately synthesize the proline-rich peptides from three ND10 fusion segments to see which one is easier to be crystallized. Meanwhile, we can attempt to use different conditions such as acetonitrile as solvent and tetrahydropyran as cosolvent (Wilhelm et al., 2014) to obtain the crystal suitable for X-ray crystallographic analysis. If the crystallography result proves the ND10 fusion segments form PPII helix structure, the next question is whether proline residues in PPII helix play a determining role in the ND10 fusion process. To test this, a recombinant virus with mutation of the proline residues need to be constructed. We can start from the mutation of prolines within the SH3 binding sites and see whether these mutations can abolish the ND10 fusion.

What ND10 components facilitate the ND10 fusion process?

If PPII helix is critical for ND10 fusion process, a logical question is which constituents in ND10 interact with PPII helix and drive for ND10 fusion. To identify these components, subtraction mass spectrometry can be performed. Briefly, the proteins interacting with ICP0 from RHG120 (ND10-fusion competent) infected cells and RHG110 (ND10-fusion incompetent) infected cells need to be identified respectively. Subtraction of binding proteins from RHG120 sample to RHG110 sample will demonstrate the possible proteins that interact with ICP0 through ND10-ES. Then the proteins from subtraction analysis will be compared with known ND10 components. If there are a couple of potential candidates at this step, siRNA knockdown assay of each candidate or combination of siRNAs against multiple candidates can be performed to see whether depletion of any candidate has an

effect on ND10 fusion.

By answering the questions above, we can further illustrate the interaction between ICP0 and ND10 by elucidating the structure of the ICP0 ND10-ES and its biological significance. In the meantime, the cellular factors that are crucial for ND10 fusion process will be identified too. These studies are critical for finding a possible new drug target in both viral and cellular proteins to block the viral replication.

What is the ubiquitination pattern of PML I in RHG105 and RHG110 infected cells?

The mutant ICP0 lacking either arm of PML I binding domains can lead to PML I degradation with the accumulation of modified PML I, which is not shown in wild-type virus infection. We hypothesize that the modified PML I are ubiquitinated. There are two scenarios which can explain this phenomenon. First, the ubiquitin transfer and the efficiency of polyubiquitination are affected by mutant ICP0. Therefore, the monoubiquitinated and diubiquitinated PML I were accumulated. Second, the polyubiquitin linkage on PML I by ICP0 with deletion of either arm is different from that by wild-type ICP0. The mutant ICP0 probably polyubiquitinates PML I with a mixture of polyubiquitin chains and a certain fraction of polyubiquitin chains signal for proteasome degradation differently.

To test the first hypothesis, the *in vitro* polyubiquitination assay will be performed. ICP0 *in vitro* ubiquitination assay for different substrates has been described elsewhere (Boutell et al., 2011; Lilley et al., 2010). Purification of PML I protein, wild-type and mutant ICP0 is the first step. Then PML I and ICP0 will be mixed with the E1 enzyme, E2 enzyme, ubiquitin protein, ATP and buffer for ubiquitination reaction to occur. After the reaction, the ability of ICP0 mutants to form poly-ubiquitin chains was assessed by probing with

ubiquitin antibody. If there is a significant decrease of polyubiquitination by mutant ICP0, it suggests that mutant ICP0 polyubiquitinate PML I less efficiently than wild-type ICP0.

To test the second hypothesis, His-tag pull-down of PML I from RHG105 or RHG110 infected cells will be analyzed through mass spectrometry to identify the ubiquitination patterns on PML I by different mutants of ICP0. An alternative way is to construct ubiquitin mutants, such as K48R and K63R. The wild-type ubiquitin and mutant ubiquitin constructs will be transfected into PML I cell to check whether mutation of lysine residues in ubiquitin has any effect on the polyubiquitination of PML I by mutant ICP0.

If the first scenario is correct, we will be able to find the sequences that play a supportive role in the interaction between ICP0 and its corresponding E2 enzyme. If the second scenario is correct, we will for the first time prove that ICP0 can polyubiquitinate its substrates in different ubiquitin linkages. The different ubiquitin linkages caused by ICP0 may be related to its multifunctional property.

To pinpoint the sequences of the PML I C-terminus interacting with ICP0 and sequences in ICP0 ND10-ES interacting with PML I.

Residues 1-83 and residues 245-474 of ICP0 are the bipartite binding regions for interaction with PML I. Through sequence alignment, residues 386-473 within 245-474 share some homology with 1-83. Two recombinant viruses, one with deletion of residues 1-83 together with deletion of residues 386-475 and another one with the deletion of residues 1-83 along with deletion of residues 245-385, can be constructed to test whether the homologous region located within residues 245-474 of ICP0 is the PML I binding domain through Co-IP assay.

Another interesting question is the PML I sequence determining its interaction with

ICP0. Since PML I has a unique C-terminus compared with PML II, the hypothesis is that the unique sequences in PML I C-terminus mediate its interaction with ICP0. Through sequence alignment, residues of 715-798 of PML I are the homologous region of ICP0 residues 1-83. Therefore, constructs of PML I 1-798 and PML I 1-714 need to be made to map the sequences in PML I that contribute to the interaction with ICP0. With these constructs, we can test whether the homologous region in PML I regulates the interaction with ICP0 through Co-IP assay. If the homologous sequences mediate the interaction between ICP0 and PML I, they are likely also involved in recognition of other substrates.

Is there a substrate recognition mediator between ICP0 and its substrates?

Even though the physical interaction between ICP0 specific sequences with PML I or PML II can be detected, we cannot rule out that this interaction is indirect and mediated by other proteins. The hypothesis is that ICP0 may employ cellular proteins for differential recognition of its substrates. The specific sequences in ICP0 for PML binding possibly are the sequences responsible for interaction with substrate recognition proteins. Hijacking components of cellular E3 ligase complex is a common mechanism for the virus to target the inhibitory proteins. For example, non-structural protein 1 (NSP1) of rotavirus could degrade β-TrCP by associating with cellular Cullin-1 (Cul1) and Cullin-3 (Cul3) and employing RING-box protein 1 (Rbx1) E3 ligase activity to inactivate the NF-κB pathway (Ding et al., 2016).

Possibly, ICP0 usurps the machinery of cellular E3 ligase for recognition and destruction of its substrates. A mass spectrometry study performed in our lab has identified Viral protein R binding protein (VprBP) as one of ICP0 binding proteins (unpublished data from our lab). VprBP serves as the substrate recognition member of

the RING-type CRL4 ligase complex and can be usurped by viral proteins, such as Vpr and Vpx, to enhance the viral infection (Nakagawa et al., 2013). Therefore, it is appealing to hypothesize that ICP0 interacts with VprBP to differentiate its substrates. To test this, siRNA knockdown of VprBP in both PML I and PML II cell lines will be performed to see whether the depletion of VprBP has any effect on PML I or PML II degradation. Our lab has already confirmed the interaction between ICP0 and VprBP through Co-IP assay. Therefore, an alternative way to do this is to map the binding region in ICP0 to interact with VprBP and construct a virus which lacks the binding region for VprBP. Then we will use this mutant virus to see whether PML I or PML II degradation is blocked.

By answering the questions above, we will illustrate the other factors besides ICP0 sequences that regulate its E3 ligase activity. These factors possibly include the E2, binding domains in ICP0 substrates, and substrate recognition mediator. These studies will reveal the mechanism how ICP0 targets various substrates and delivers them for proteasomal degradation, which is critical for understanding ICP0 coordination of its multifunction.

REFERENCES

Adzhubei, A. A.et al. (2013). Polyproline-II helix in proteins: structure and function. *J Mol Biol, 425*(12), 2100-2132. doi: 10.1016/j.jmb.2013.03.018

Arnold, M. M. (2016). The Rotavirus Interferon Antagonist NSP1: Many Targets, Many Questions. *J Virol, 90*(11), 5212-5215. doi: 10.1128/JVI.03068-15

Ascoli, C. A., and Maul, G. G. (1991). Identification of a novel nuclear domain. *J Cell Biol, 112*(5), 785-795.

Bacarizo, J.et al. (2015). Structure of the c-Src-SH3 domain in complex with a proline-rich motif of NS5A protein from the hepatitis C virus. *J Struct Biol, 189*(1), 67-72. doi: 10.1016/j.jsb.2014.11.004

Batterson, W.et al. (1983). Molecular genetics of herpes simplex virus. VIII. further characterization of a temperature-sensitive mutant defective in release of viral DNA and in other stages of the viral reproductive cycle. *J Virol, 45*(1), 397-407.

Bernardi, R., and Pandolfi, P. P. (2003). Role of PML and the PML-nuclear body in the control of programmed cell death. *Oncogene, 22*(56), 9048-9057. doi: 10.1038/sj.onc.1207106

Bernardi, R., and Pandolfi, P. P. (2007). Structure, dynamics and functions of promyelocytic leukaemia nuclear bodies. *Nat Rev Mol Cell Biol, 8*(12), 1006-1016. doi: 10.1038/nrm2277

Bloom, D. C.et al. (2010). Epigenetic regulation of latent HSV-1 gene expression. *Biochim Biophys Acta, 1799*(3-4), 246-256. doi: 10.1016/j.bbagrm.2009.12.001

Boutell, C.et al. (2005). Reciprocal activities between herpes simplex virus type 1

regulatory protein ICP0, a ubiquitin E3 ligase, and ubiquitin-specific protease

USP7. *J Virol, 79*(19), 12342-12354. doi: 10.1128/JVI.79.19.12342-12354.2005

Boutell, C.et al. (2011). A viral ubiquitin ligase has substrate preferential SUMO targeted

ubiquitin ligase activity that counteracts intrinsic antiviral defence. *PLoS Pathog,

7*(9), e1002245. doi: 10.1371/journal.ppat.1002245

Boutell, C.et al. (2008). Herpes simplex virus type 1 ICP0 phosphorylation mutants

impair the E3 ubiquitin ligase activity of ICP0 in a cell type-dependent manner. *J

Virol, 82*(21), 10647-10656. doi: 10.1128/JVI.01063-08

Boutell, C., and Everett, R. D. (2013). Regulation of alphaherpesvirus infections by the

ICP0 family of proteins. *J Gen Virol, 94*(Pt 3), 465-481. doi:

10.1099/vir.0.048900-0

Boutell, C.et al. (2002). Herpes simplex virus type 1 immediate-early protein ICP0 and is

isolated RING finger domain act as ubiquitin E3 ligases in vitro. *J Virol, 76*(2),

841-850.

Canning, M.et al. (2004). A RING finger ubiquitin ligase is protected from autocatalyzed

ubiquitination and degradation by binding to ubiquitin-specific protease USP7. *J

Biol Chem, 279*(37), 38160-38168. doi: 10.1074/jbc.M402885200

Chee, A. V.et al. (2003). Promyelocytic leukemia protein mediates interferon-based anti-

herpes simplex virus 1 effects. *J Virol, 77*(12), 7101-7105.

Chelbi-Alix, M. K., and de The, H. (1999). Herpes virus induced proteasome-dependent

degradation of the nuclear bodies-associated PML and Sp100 proteins.

Oncogene, 18(4), 935-941. doi: 10.1038/sj.onc.1202366

Chelbi-Alix, M. K.et al. (1998). Resistance to virus infection conferred by the interferon-induced promyelocytic leukemia protein. *J Virol, 72*(2), 1043-1051.

Chen, J., and Silverstein, S. (1992). Herpes simplex viruses with mutations in the gene encoding ICP0 are defective in gene expression. *J Virol, 66*(5), 2916-2927.

Chen, J. X.et al. (1991). Mutational analysis of the sequence encoding ICP0 from herpes simplex virus type 1. *Virology, 180*(1), 207-220.

Cliffe, A. R., and Knipe, D. M. (2008). Herpes simplex virus ICP0 promotes both histone removal and acetylation on viral DNA during lytic infection. *J Virol, 82*(24), 12030-12038. doi: 10.1128/JVI.01575-08

Cliffe, A. R., and Wilson, A. C. (2017). Restarting Lytic Gene Transcription at the Onset of Herpes Simplex Virus Reactivation. *J Virol, 91*(2). doi: 10.1128/JVI.01419-16

Condemine, W.et al. (2007). A nucleolar targeting signal in PML-I addresses PML to nucleolar caps in stressed or senescent cells. *J Cell Sci, 120*(Pt 18), 3219-3227. doi: 10.1242/jcs.007492

Costanzo, F.et al. (1977). Evidence that herpes simplex virus DNA is transcribed by cellular RNA polymerase B. *J Virol, 21*(3), 996-1001.

Cuchet-Lourenco, D.et al. (2012). Herpes simplex virus 1 ubiquitin ligase ICP0 interacts with PML isoform I and induces its SUMO-independent degradation. *J Virol, 86*(20), 11209-11222. doi: 10.1128/JVI.01145-12

Cuchet, D.et al. (2011). PML isoforms I and II participate in PML-dependent restriction of HSV-1 replication. *J Cell Sci, 124*(Pt 2), 280-291. doi: 10.1242/jcs.075390

Decorsiere, A.et al. (2016). Hepatitis B virus X protein identifies the Smc5/6 complex as a host restriction factor. *Nature, 531*(7594), 386-389. doi: 10.1038/nature17170

Deng, L.et al. (2000). Activation of the IkappaB kinase complex by TRAF6 requires a dimeric ubiquitin-conjugating enzyme complex and a unique polyubiquitin chain. *Cell, 103*(2), 351-361.

di Masi, A.et al. (2016). PML nuclear body disruption impairs DNA double-strand break sensing and repair in APL. *Cell Death Dis, 7*, e2308. doi: 10.1038/cddis.2016.115

Ding, S.et al. (2016). Comparative Proteomics Reveals Strain-Specific beta-TrCP Degradation via Rotavirus NSP1 Hijacking a Host Cullin-3-Rbx1 Complex. *PLoS Pathog, 12*(10), e1005929. doi: 10.1371/journal.ppat.1005929

Everett, R.et al. (1995). Point mutations in the herpes simplex virus type 1 Vmw110 RING finger helix affect activation of gene expression, viral growth, and interaction with PML-containing nuclear structures. *J Virol, 69*(11), 7339-7344.

Everett, R. D. (1987). A detailed mutational analysis of Vmw110, a trans-acting transcriptional activator encoded by herpes simplex virus type 1. *EMBO J, 6*(7), 2069-2076.

Everett, R. D.et al. (2014). Sequences related to SUMO interaction motifs in herpes simplex virus 1 protein ICP0 act cooperatively to stimulate virus infection. *J Virol, 88*(5), 2763-2774. doi: 10.1128/JVI.03417-13

Everett, R. D., and Chelbi-Alix, M. K. (2007). PML and PML nuclear bodies: implications in antiviral defence. *Biochimie, 89*(6-7), 819-830. doi: 10.1016/j.biochi.2007.01.004

Everett, R. D.et al. (1998). The disruption of ND10 during herpes simplex virus infection correlates with the Vmw110- and proteasome-dependent loss of several PML isoforms. *J Virol, 72*(8), 6581-6591.

Everett, R. D., and Maul, G. G. (1994). HSV-1 IE protein Vmw110 causes redistribution of PML. *EMBO J, 13*(21), 5062-5069.

Everett, R. D.et al. (2008). Replication of ICP0-null mutant herpes simplex virus type 1 is restricted by both PML and Sp100. *J Virol, 82*(6), 2661-2672. doi: 10.1128/JVI.02308-07

Everett, R. D.et al. (2006). PML contributes to a cellular mechanism of repression of herpes simplex virus type 1 infection that is inactivated by ICP0. *J Virol, 80*(16), 7995-8005. doi: 10.1128/JVI.00734-06

Freemont, P. S. (2000). RING for destruction? *Curr Biol, 10*(2), R84-87.

Glass, M., and Everett, R. D. (2013). Components of promyelocytic leukemia nuclear bodies (ND10) act cooperatively to repress herpesvirus infection. *J Virol, 87*(4), 2174-2185. doi: 10.1128/JVI.02950-12

Greene, W.et al. (2012). The ubiquitin/proteasome system mediates entry and endosomal trafficking of Kaposi's sarcoma-associated herpesvirus in endothelial cells. *PLoS Pathog, 8*(5), e1002703. doi: 10.1371/journal.ppat.1002703

Gu, H. (2016). Infected cell protein 0 functional domains and their coordination in herpes simplex virus replication. *World J Virol, 5*(1), 1-13. doi: 10.5501/wjv.v5.i1.1

Gu, H.et al. (2005). Components of the REST/CoREST/histone deacetylase repressor complex are disrupted, modified, and translocated in HSV-1-infected cells. *Proc Natl Acad Sci U S A, 102*(21), 7571-7576. doi: 10.1073/pnas.0502658102

Gu, H.et al. (2009). During its nuclear phase the multifunctional regulatory protein ICP0 undergoes proteolytic cleavage characteristic of polyproteins. *Proc Natl Acad Sci U S A, 106*(45), 19132-19137. doi: 10.1073/pnas.0910920106

Gu, H., and Roizman, B. (2009). The two functions of herpes simplex virus 1 ICP0, inhibition of silencing by the CoREST/REST/HDAC complex and degradation of PML, are executed in tandem. *J Virol, 83*(1), 181-187. doi: 10.1128/JVI.01940-08

Gu, H., and Zheng, Y. (2016). Role of ND10 nuclear bodies in the chromatin repression of HSV-1. *Virol J, 13*, 62. doi: 10.1186/s12985-016-0516-4

Gu, H.et al. (2013). Interaction of herpes simplex virus ICP0 with ND10 bodies: a sequential process of adhesion, fusion, and retention. *J Virol, 87*(18), 10244-10254. doi: 10.1128/JVI.01487-13

Henderson, B. R., and Eleftheriou, A. (2000). A comparison of the activity, sequence specificity, and CRM1-dependence of different nuclear export signals. *Exp Cell Res, 256*(1), 213-224. doi: 10.1006/excr.2000.4825

Herrera, F. J., and Triezenberg, S. J. (2004). VP16-dependent association of chromatin-modifying coactivators and underrepresentation of histones at immediate-early gene promoters during herpes simplex virus infection. *J Virol, 78*(18), 9689-9696. doi: 10.1128/JVI.78.18.9689-9696.2004

Ho, D. Y., and Mocarski, E. S. (1989). Herpes simplex virus latent RNA (LAT) is not required for latent infection in the mouse. *Proc Natl Acad Sci U S A, 86*(19), 7596-7600.

Honess, R. W., and Roizman, B. (1974). Regulation of herpesvirus macromolecular synthesis. I. Cascade regulation of the synthesis of three groups of viral proteins. *J Virol, 14*(1), 8-19.

Hrecka, K.et al. (2011). Vpx relieves inhibition of HIV-1 infection of macrophages mediated by the SAMHD1 protein. *Nature, 474*(7353), 658-661. doi: 10.1038/nature10195

Jensen, K.et al. (2001). PML protein isoforms and the RBCC/TRIM motif. *Oncogene, 20*(49), 7223-7233. doi: 10.1038/sj.onc.1204765

Jul-Larsen, A.et al. (2010). Subcellular distribution of nuclear import-defective isoforms of the promyelocytic leukemia protein. *BMC Mol Biol, 11*, 89. doi: 10.1186/1471-2199-11-89

Kalamvoki, M.et al. (2012). Overexpression of the ubiquitin-specific protease 7 resulting from transfection or mutations in the ICP0 binding site accelerates rather than depresses herpes simplex virus 1 gene expression. *J Virol, 86*(23), 12871-12878. doi: 10.1128/JVI.01981-12

Kelly, B. J.et al. (2009). Functional roles of the tegument proteins of herpes simplex virus type 1. *Virus Res, 145*(2), 173-186. doi: 10.1016/j.virusres.2009.07.007

Kim, J. Y.et al. (2012). Transient reversal of episome silencing precedes VP16-dependent transcription during reactivation of latent HSV-1 in neurons. *PLoS Pathog, 8*(2), e1002540. doi: 10.1371/journal.ppat.1002540

Kim, Y. E., and Ahn, J. H. (2015). Positive role of promyelocytic leukemia protein in type I interferon response and its regulation by human cytomegalovirus. *PLoS Pathog, 11*(3), e1004785. doi: 10.1371/journal.ppat.1004785

Kirui, J.et al. (2016). Ubiquitination up-regulates influenza virus polymerase function. *J Virol.* doi: 10.1128/JVI.01829-16

Knipe, D. M., and Cliffe, A. (2008). Chromatin control of herpes simplex virus lytic and latent infection. *Nat Rev Microbiol, 6*(3), 211-221. doi: 10.1038/nrmicro1794

Kristensson, K.et al. (1986). Neuritic transport of herpes simplex virus in rat sensory neurons in vitro. Effects of substances interacting with microtubular function and axonal flow [nocodazole, taxol and erythro-9-3-(2-hydroxynonyl)adenine]. *J Gen Virol, 67 (Pt 9)*, 2023-2028. doi: 10.1099/0022-1317-67-9-2023

Lallemand-Breitenbach, V., and de The, H. (2010). PML nuclear bodies. *Cold Spring Harb Perspect Biol, 2*(5), a000661. doi: 10.1101/cshperspect.a000661

Lang, M.et al. (2010). Three-dimensional organization of promyelocytic leukemia nuclear bodies. *J Cell Sci, 123*(Pt 3), 392-400. doi: 10.1242/jcs.053496

Lavau, C.et al. (1995). The acute promyelocytic leukaemia-associated PML gene is induced by interferon. *Oncogene, 11*(5), 871-876.

Lees-Miller, S. P.et al. (1996). Attenuation of DNA-dependent protein kinase activity and its catalytic subunit by the herpes simplex virus type 1 transactivator ICP0. *J Virol, 70*(11), 7471-7477.

Li, B.et al. (2007). The role of chromatin during transcription. *Cell, 128*(4), 707-719. doi: 10.1016/j.cell.2007.01.015

Liang, Y.et al. (2005). Herpes simplex virus 1 infected cell protein 0 forms a complex with CIN85 and Cbl and mediates the degradation of EGF receptor from cell surfaces. *Proc Natl Acad Sci U S A, 102*(16), 5838-5843. doi: 10.1073/pnas.0501253102

Lilley, C. E.et al. (2005). DNA repair proteins affect the lifecycle of herpes simplex virus 1. *Proc Natl Acad Sci U S A, 102*(16), 5844-5849. doi: 10.1073/pnas.0501916102

Lilley, C. E.et al. (2011). The intrinsic antiviral defense to incoming HSV-1 genomes includes specific DNA repair proteins and is counteracted by the viral protein ICP0. *PLoS Pathog, 7*(6), e1002084. doi: 10.1371/journal.ppat.1002084

Lilley, C. E.et al. (2010). A viral E3 ligase targets RNF8 and RNF168 to control histone ubiquitination and DNA damage responses. *EMBO J, 29*(5), 943-955. doi: 10.1038/emboj.2009.400

Lomonte, P.et al. (2004). Functional interaction between class II histone deacetylases and ICP0 of herpes simplex virus type 1. *J Virol, 78*(13), 6744-6757. doi: 10.1128/JVI.78.13.6744-6757.2004

Maroui, M. A.et al. (2011). Promyelocytic leukemia isoform IV confers resistance to encephalomyocarditis virus via the sequestration of 3D polymerase in nuclear bodies. *J Virol, 85*(24), 13164-13173. doi: 10.1128/JVI.05808-11

Maul, G. G., and Everett, R. D. (1994). The nuclear location of PML, a cellular member of the C3HC4 zinc-binding domain protein family, is rearranged during herpes simplex virus infection by the C3HC4 viral protein ICP0. *J Gen Virol, 75 (Pt 6)*, 1223-1233. doi: 10.1099/0022-1317-75-6-1223

Maul, G. G.et al. (1993). Modification of discrete nuclear domains induced by herpes simplex virus type 1 immediate early gene 1 product (ICP0). *J Gen Virol, 74 (Pt 12)*, 2679-2690. doi: 10.1099/0022-1317-74-12-2679

Maul, G. G.et al. (1996). Nuclear domain 10 as preexisting potential replication start sites of herpes simplex virus type-1. *Virology, 217*(1), 67-75. doi: 10.1006/viro.1996.0094

Melroe, G. T.et al. (2007). Recruitment of activated IRF-3 and CBP/p300 to herpes simplex virus ICP0 nuclear foci: Potential role in blocking IFN-beta induction. *Virology, 360*(2), 305-321. doi: 10.1016/j.virol.2006.10.028

Meredith, M.et al. (1995). Separation of sequence requirements for HSV-1 Vmw110 multimerisation and interaction with a 135-kDa cellular protein. *Virology, 209*(1), 174-187. doi: 10.1006/viro.1995.1241

Meyer, H. J., and Rape, M. (2014). Enhanced protein degradation by branched ubiquitin chains. *Cell, 157*(4), 910-921. doi: 10.1016/j.cell.2014.03.037

Mitchell, R. S.et al. (2009). Vpu antagonizes BST-2-mediated restriction of HIV-1 release via beta-TrCP and endo-lysosomal trafficking. *PLoS Pathog, 5*(5), e1000450. doi: 10.1371/journal.ppat.1000450

Mohni, K. N.et al. (2011). DNA mismatch repair proteins are required for efficient herpes simplex virus 1 replication. *J Virol, 85*(23), 12241-12253. doi: 10.1128/JVI.05487-11

Mossman, K. L.et al. (2000). Herpes simplex virus ICP0 mutants are hypersensitive to interferon. *J Virol, 74*(4), 2052-2056.

Murphy, C. M.et al. (2016). Hepatitis B Virus X Protein Promotes Degradation of SMC5/6 to Enhance HBV Replication. *Cell Rep, 16*(11), 2846-2854. doi: 10.1016/j.celrep.2016.08.026

Musacchio, A.et al. (1994). High-resolution crystal structures of tyrosine kinase SH3 domains complexed with proline-rich peptides. *Nat Struct Biol, 1*(8), 546-551.

Nakagawa, T.et al. (2013). VprBP (DCAF1): a promiscuous substrate recognition subunit that incorporates into both RING-family CRL4 and HECT-family EDD/UBR5 E3 ubiquitin ligases. *BMC Mol Biol, 14*, 22. doi: 10.1186/1471-2199-14-22

Negorev, D., and Maul, G. G. (2001). Cellular proteins localized at and interacting within ND10/PML nuclear bodies/PODs suggest functions of a nuclear depot. *Oncogene, 20*(49), 7234-7242. doi: 10.1038/sj.onc.1204764

Nguyen, L. A.et al. (2005). Physical and functional link of the leukemia-associated factors AML1 and PML. *Blood, 105*(1), 292-300. doi: 10.1182/blood-2004-03-1185

Oh, J., and Fraser, N. W. (2008). Temporal association of the herpes simplex virus genome with histone proteins during a lytic infection. *J Virol, 82*(7), 3530-3537. doi: 10.1128/JVI.00586-07

Ohsaki, Y.et al. (2016). PML isoform II plays a critical role in nuclear lipid droplet formation. *J Cell Biol, 212*(1), 29-38. doi: 10.1083/jcb.201507122

Orzalli, M. H.et al. (2013). Nuclear interferon-inducible protein 16 promotes silencing of herpesviral and transfected DNA. *Proc Natl Acad Sci U S A, 110*(47), E4492-4501. doi: 10.1073/pnas.1316194110

Orzalli, M. H.et al. (2012). Nuclear IFI16 induction of IRF-3 signaling during herpesviral infection and degradation of IFI16 by the viral ICP0 protein. *Proc Natl Acad Sci U S A, 109*(44), E3008-3017. doi: 10.1073/pnas.1211302109

Ott, D. E.et al. (1998). Ubiquitin is covalently attached to the p6Gag proteins of human immunodeficiency virus type 1 and simian immunodeficiency virus and to the p12Gag protein of Moloney murine leukemia virus. *J Virol, 72*(4), 2962-2968.

Patnaik, A.et al. (2000). Ubiquitin is part of the retrovirus budding machinery. *Proc Natl Acad Sci U S A, 97*(24), 13069-13074. doi: 10.1073/pnas.97.24.13069

Perez-Caballero, D.et al. (2009). Tetherin inhibits HIV-1 release by directly tethering virions to cells. *Cell, 139*(3), 499-511. doi: 10.1016/j.cell.2009.08.039

Pickart, C. M., and Eddins, M. J. (2004). Ubiquitin: structures, functions, mechanisms. *Biochim Biophys Acta, 1695*(1-3), 55-72. doi: 10.1016/j.bbamcr.2004.09.019

Rath, A.et al. (2005). The structure of "unstructured" regions in peptides and proteins: role of the polyproline II helix in protein folding and recognition. *Biopolymers, 80*(2-3), 179-185. doi: 10.1002/bip.20227

Regad, T.et al. (2001). PML mediates the interferon-induced antiviral state against a complex retrovirus via its association with the viral transactivator. *EMBO J, 20*(13), 3495-3505. doi: 10.1093/emboj/20.13.3495

Roizman, B.et al. (2013). Herpes Simplex Virus. In B. N. Fields, D. M. Knipe, & P. M. Howley (Eds.), *Fields virology* (6th ed.). Philadelphia: Wolters Kluwer Health/Lippincott Williams & Wilkins.

Salomoni, P., and Pandolfi, P. P. (2002). The role of PML in tumor suppression. *Cell, 108*(2), 165-170.

Sato, Y.et al. (2016). Cellular Transcriptional Coactivator RanBP10 and Herpes Simplex Virus 1 ICP0 Interact and Synergistically Promote Viral Gene Expression and Replication. *J Virol, 90*(6), 3173-3186. doi: 10.1128/JVI.03043-15

Sette, P.et al. (2013). Ubiquitin conjugation to Gag is essential for ESCRT-mediated HIV-1 budding. *Retrovirology, 10*, 79. doi: 10.1186/1742-4690-10-79

Siligardi, G., and Drake, A. F. (1995). The importance of extended conformations and, in particular, the PII conformation for the molecular recognition of peptides. *Biopolymers, 37*(4), 281-292. doi: 10.1002/bip.360370406

Smith, S., and Weller, S. K. (2015). HSV-I and the cellular DNA damage response. *Future Virol, 10*(4), 383-397. doi: 10.2217/fvl.15.18

Stehmeier, P., and Muller, S. (2009). Phospho-regulated SUMO interaction modules connect the SUMO system to CK2 signaling. *Mol Cell, 33*(3), 400-409. doi: 10.1016/j.molcel.2009.01.013

Tavalai, N., and Stamminger, T. (2008). New insights into the role of the subnuclear structure ND10 for viral infection. *Biochim Biophys Acta, 1783*(11), 2207-2221. doi: 10.1016/j.bbamcr.2008.08.004

Turvey, S. E., and Broide, D. H. (2010). Innate immunity. *J Allergy Clin Immunol, 125*(2 Suppl 2), S24-32. doi: 10.1016/j.jaci.2009.07.016

Uprichard, S. L., and Knipe, D. M. (1997). Assembly of herpes simplex virus replication proteins at two distinct intranuclear sites. *Virology, 229*(1), 113-125. doi: 10.1006/viro.1996.8430

Van Damme, E.et al. (2010). A manually curated network of the PML nuclear body interactome reveals an important role for PML-NBs in SUMOylation dynamics. *Int J Biol Sci, 6*(1), 51-67.

Wang, Q. Y.et al. (2005). Herpesviral latency-associated transcript gene promotes assembly of heterochromatin on viral lytic-gene promoters in latent infection.

Proc Natl Acad Sci U S A, 102(44), 16055-16059. doi: 10.1073/pnas.0505850102

Wang, S.et al. (2016). The ubiquitin-proteasome system is essential for the productive entry of Japanese encephalitis virus. *Virology, 498*, 116-127. doi: 10.1016/j.virol.2016.08.013

Weidtkamp-Peters, S.et al. (2008). Dynamics of component exchange at PML nuclear bodies. *J Cell Sci, 121*(Pt 16), 2731-2743. doi: 10.1242/jcs.031922

Welchman, R. L.et al. (2005). Ubiquitin and ubiquitin-like proteins as multifunctional signals. *Nat Rev Mol Cell Biol, 6*(8), 599-609. doi: 10.1038/nrm1700

Wilhelm, P.et al. (2014). A crystal structure of an oligoproline PPII-helix, at last. *J Am Chem Soc, 136*(45), 15829-15832. doi: 10.1021/ja507405j

WuDunn, D., and Spear, P. G. (1989). Initial interaction of herpes simplex virus with cells is binding to heparan sulfate. *J Virol, 63*(1), 52-58.

Wysocka, J., and Herr, W. (2003). The herpes simplex virus VP16-induced complex: the makings of a regulatory switch. *Trends Biochem Sci, 28*(6), 294-304. doi: 10.1016/S0968-0004(03)00088-4

Xu, P.et al. (2016). PML plays both inimical and beneficial roles in HSV-1 replication. *Proc Natl Acad Sci U S A, 113*(21), E3022-3028. doi: 10.1073/pnas.1605513113

Yan, N., and Chen, Z. J. (2012). Intrinsic antiviral immunity. *Nat Immunol, 13*(3), 214-222. doi: 10.1038/ni.2229

Yau, R., and Rape, M. (2016). The increasing complexity of the ubiquitin code. *Nat Cell Biol, 18*(6), 579-586. doi: 10.1038/ncb3358

Zheng, N., and Shabek, N. (2017). Ubiquitin Ligases: Structure, Function, and

Regulation. *Annu Rev Biochem*. doi: 10.1146/annurev-biochem-060815-014922

Zheng, Y., and Gu, H. (2015). Identification of three redundant segments responsible for

herpes simplex virus 1 ICP0 to fuse with ND10 nuclear bodies. *J Virol, 89*(8),

4214-4226. doi: 10.1128/JVI.03658-14

Zheng, Y.et al. (2016). A Tale of Two PMLs: Elements Regulating a Differential

Substrate Recognition by the ICP0 E3 Ubiquitin Ligase of Herpes Simplex Virus

1. *J Virol, 90*(23), 10875-10885. doi: 10.1128/JVI.01636-16

Zhong, S.et al. (2000). The transcriptional role of PML and the nuclear body. *Nat Cell

Biol, 2*(5), E85-90. doi: 10.1038/35010583

ABSTRACT

TARGETING HOST DEFENSE: THE DYNAMIC ND10 INTERACTION AND THE DIFFERENTIAL SUBSTRATE RECOGNITION OF HSV-1 ICP0

by

YI ZHENG

AUGUST 2017

Advisor: Dr. Haidong Gu

Major: Biological Sciences

Degree: Doctor of Philosophy

ICP0 is one of the immediate early viral proteins and essential for HSV-1 replication in low MOI infection. ICP0 is involved in manipulating various cellular pathways and attenuating their inhibitory functions on viral replication through either protein-protein interaction or using its E3 ligase activity to degrade restrictive factors. Upon infection, HSV-1 viral DNA is injected into the nucleus and found to be closely associated with ND10. ND10 association with viral DNA causes the repression of viral gene expression, which is inactivated by ICP0. HSV-1 employs ICP0 to target key ND10 components PML and Sp100 for proteasomal degradation, leading to the destruction of ND10 and dispersion of inhibitory ND10 components. Therefore, viral gene expression and viral replication are enhanced.

First, I investigated the ICP0 dynamic interaction with ND10, especially the ND10 fusion step. ND10 fusion step is presumably regulating ICP0 access to its substrate and hence critical for ICP0 to execute its function. Through deletion mapping and confocal microscopy, I have identified three redundant and proline-rich segments in ICP0 that independently drive ICP0 to fuse with ND10. This study is the necessary groundwork for

understanding the protein-protein interaction during ND10 fusion.

Next, I identified the elements in ICP0 that control its substrate recognition, especially differential degradation of PML isoforms. Through deletion mapping and half-life assay, I have identified ICP0 uses at least two different mechanisms for targeting PML isoforms. This study helps to understand the sequences in ICP0 that are essential for its substrate differentiation and regulation of its E3 ubiquitin ligase activity.

Overall, I have identified the sequences in ICP0 governing interaction between ICP0 and ND10 and regulating degradation of ND10 components through both studies. These studies laid the foundation for understanding ICP0 coordination of its multifunction and provide critical and novel information for designing possible drug targets to block HSV-1 infection.

AUTOBIOGRAPHICAL STATEMENT

YI ZHENG

EDUCATION:

2011-2017   PhD in Biology, Wayne State University, Detroit, USA
2006-2011   BS in Veterinary Medicine, Huazhong Agricultural University, Wuhan, China

PUBLICATIONS:

Zheng Y, Samrat SK, Gu H (2016). A Tale of Two PMLs: Elements Regulating a Differential Substrate Recognition by the ICP0 E3 Ubiquitin Ligase of Herpes Simplex Virus 1. J Virol. 90(23):10875-85.
Gu H, **Zheng Y** (2016). Role of ND10 nuclear bodies in the chromatin repression of HSV-1. Virol J. 13(1):62.
Zheng Y, Gu H (2015). Identification of Three Redundant Segments Responsible for Herpes Simplex Virus 1 Infected Cell Protein 0 to Fuse with ND10 Nuclear Bodies. J Virol. 89(8):4214-26.
Gu H, **Zheng Y**, Roizman B (2013). Interaction of Herpes Simplex Virus ICP0 with ND10 Bodies: a Sequential Process of Adhesion, Fusion, and Retention. J Virol. 87(18):10244-54.

HONORS AND AWARDS:

2016: 35th Annual Meeting of the American Society for Virology Travel Award
       P. Dennis Smith Award for Genetics
       Graduate and Postdoctoral Research Symposium 1st place presentation Award

2015: Exceptional Graduate Research Assistant
       Thomas C. Rumble Graduate Fellowship
       Graduate Exhibition 3rd place presentation award